Electrophysiological Assessment of Two Potential hERG Correctors

Joshua Solomon, Department of Physiology, McGill University, Montreal

June 2017

A thesis submitted to McGill University in partial fulfillment of the requirements of the degree of Master's of Science

Table of Contents

Abstract (English)

Mutations of the **h**uman ***E**ther-à-go-go-***R**elated **G**ene (hERG) potassium channel prolong cardiac ventricular repolarization, which presents clinically as Long QT Syndrome. Ventricular arrhythmias result from the misfolding of hERG at the endoplasmic reticulum (ER), and impaired trafficking to the cell surface. An independent high throughput screen identified 153 compounds that up-regulate hERG levels at the cell surface in both wild-type (WT) and selected hERG mutants. Consequently, these drugs might provide therapeutic tools for treating Long QT Syndrome. Further screening experiments, to rule out block of the hERG channel pore, reduced the list to two candidate compounds that cause significant up-regulation of hERG: 5,6-dichloro-3-ethyl-1H-benzoimidazol-2-one (DCEBIO), a potassium channel activatior, and anagrelide, usind in the treatment of thrombocytosis. To determine whether these candidate drugs can rescue wild-type hERG expression and gating properties of various hERG mutants a functional analysis was performed using the whole-cell patch clamp technique. This electrophysiological approach provides information concerning both hERG current magnitude and channel gating kinetics. In the present study, it is shown that overnight treatment with either DCEBIO or anagrelide significantly increase functional cell-surface hERG in HeLa cell populations expressing WT and various hERG mutants. However, neither drug was capable of rescuing defective gating of hERG mutants. These results demonstrate that it is possible for drugs to increase functional expression of hERG mutants by increasing cell surface expression without affecting hERG gating.

Abstract (French)

Les mutations du canal de potassium génétique humain (HERG) de Ether-à-go-go prolongent la repolarisation du ventricule cardiaque, qui se présente cliniquement comme un syndrome de QT prolongé. Les arythmies ventriculaires résultent du repliement de hERG au réticulum endoplasmique (ER) et entravent le trafic sur la surface de la cellule. Un écran indépendant à haut débit a identifié 153 composés qui régule les niveaux de HERG à la surface de la cellule dans des mutants hERG (WT) et de type sauvage sélectionnés. Par conséquent, ces médicaments peuvent fournir des outils thérapeutiques pour traiter le syndrome du QT long. D'autres expériences de dépistage, pour exclure le blocage du pore du canal hERG, ont réduit la liste à deux composés candidats qui provoquent une régulation significative de la hERG: 5,6-dichloro-3-éthyl-lH-benzoimidazol-2-one (DCEBIO) , Un activateur de canal de potassium, et anagrelide, usind dans le traitement de la thrombocytose. Pour déterminer si ces médicaments candidats peuvent sauver des propriétés d'expression et de gating de type sauvage de divers mutants hERG, une analyse fonctionnelle a été effectuée en utilisant la technique de la pince de patch à cellules entières. Cette approche électrophysiologique fournit des informations concernant à la fois la magnitude actuelle et la cinétique de canalisation. Dans la présente étude, il est démontré que le traitement pendant la nuit avec DCEBIO ou anagrelide augmente de manière significative le HERG fonctionnel de la surface cellulaire dans les populations de cellules HeLa exprimant WT et divers mutants hERG. Cependant, aucun médicament n'était capable de sauver des gingissements défectueux de mutants hERG. Ces résultats démontrent qu'il est possible que les médicaments augmentent l'expression fonctionnelle des mutants hERG en augmentant l'expression de la surface cellulaire sans affecter le déclenchement hERG.

Introduction

Translation of the KCNH2 gene produces the *human ether-a-go-go related gene* (hERG), the pore-forming subunit of a delayed rectifier voltage-gated K^+ (VGK) ion channel (Abbott *et al*. 1999). The fully formed channel is comprised of four channel subunits ($K_v11.1$), each containing six transmembrane segments (S1-S6). Although found in many tissues, hERG is best characterized for it's role in cardiac cells and the coordination of cardiac physiology (Warmke *et al.* 1994). The fully assembled VGK channel is responsible for the rapid component of the delayed rectifier K^+ current (I_{Kr}). A functional channel can exist in one of three gating states: *closed*, *open*, or *inactivated*. Like other voltage-gated K^+ channels, hERG contains several positive charges in its S4 domain which act as a primary voltage sensor for channel opening (Piper *et al.* 2005; Subbiah *et al*. 2004). However, unlike most other ion channels, $K_v11.1$ possesses many unique kinetic properties. For instance, $K_v11.1$ rates of inactivation are observed to be much faster than its kinetics of activation (Schonherr *et al.* 1996; Smith *et al*. 1996).

Owing to $K_v11.1$ slow activation and deactivation kinetics in conjunction with rapid voltage-dependent inactivation, $K_v11.1$ is the major determinant of the duration of the plateau phase in the cardiac action potential (Smith *et al.* 1996; Sanguinetti *et al.* 2006). Proper coordination of the plateau phase is essential for ensuring that cardiac myocytes have sufficient time to release Ca^{2+} via I_{CaL} and NCX1 (Dong *et al*. 2002). At the onset of repolarization of cardiac myocytes, I_{Kr} begins to recover from inactivation, thus passing more current and quickening repolarization, leading to a greater recovery from inactivation. This positive feedback loop is crucial in permitting repolarization to be rapid and robust. Together, this highlights the importance of the unique gating properties of $K_v11.1$ channels.

Mutations in KCNH2 can have harmful consequences on cardiac electrical activity due to its crucial role in determining the duration of the cardiac action potential. A reduction in functional expression of hERG can delay cardiac repolarization and lead to the development of cardiac arrhythmias (Curran *et al.* 1995). Impaired functional expression of hERG is linked to Long-QT Syndrome Type 2 (LQT2), characterized by delayed repolarization of the cardiac action potential. LQT2 may lead to *Torsades de Pointes*, palpitations, and sudden cardiac death (Chiamvimonvat *et al* 2016). The magnitude of current which a given ion channel passes depends equally on the *total number of channels at the cell surface*, the probability that the given channel is open, transmembrane voltage, and single-channel conductance (Vanderberg *et al.* 2012). Since loss of function mutations of hERG may cause reduction alter several of these conductance properties, these mutations often lead to a reduction in current; as seen in LQT2. Previous studies revealed that abnormal trafficking of misfolded hERG to the cell surface is the primary cause for LQT2 (Foo *et al.* 2015; Zhou, Going, Eptein *et al*. 1998).

Several LQT2-associated mutations in the hERG N-terminal Per-Arnt-Sim (PAS) domain are thought to disrupt channel folding. Misfolded channels are recognized by the ER protein quality control machinery, leading to ER retention, retrotranslocation from the ER membrane and proteosomal degradation. This causes impaired biosynthesis and reduced plasma membrane (PM) expression (Harley et al., 2012; Paulussen et al. 2002). At the PM, misfolded hERG channels are subject to another round of quality control involving rapid internalization, impaired endocytic recycling and delivery to lysosomes (Apaja *et al.* 2013). Most PAS mutations also accelerate $K_v11.1$ deactivation; however, these channels retain at least partial function (Ke *et al.* 2013), making rescue of hERG trafficking and/or PM stability via pharmacochaperones a

promising therapeutic option (Rajamani *et al.* 2002).

Recently, Brian Foo, a fellow graduate student in the Shrier lab, performed a high throughput cell surface ELISA screen using externally HA-tagged hERG (stably expressing HeLa cells) to evaluate the effects of compounds from a 5000 compound library (BioActive compound library) on the plasma membrane expression of WT hERG. The preliminary screen identified 153 compounds that upregulate the abundance of WT hERG channels at the cell surface. A further screen was conducted with a selected group of upregulators, using a PAS domain hERG mutant channel and a hERG mutant channel with a modified pore drug binding site (Sanguinetti & Tristani-Firouzi 2006) to determine a subset of drugs that upregulate PAS domain mutant channel expression. This is screen also identified candidates with a low probability of binding the channel pore. However, there is a need to verify directly whether any of these compounds can correct mutant hERG channel expression without blocking the channel pore or affecting channel kinetics.

The aim of the current study is to characterize the functionality of $K_v11.1$ channels following upregulation induced by compounds identified in the aforementioned screen. It has been shown that many hERG activators alter channel kinetics (Perry *et al.* 2010). Rescue of the kinetic defects observed in hERG PAS domain mutants could be one possible mechanism of rescue of channel function, and ultimately LQT2. However, in addition to rescuing altered channel kinetics, exclusive rescue of channel trafficking has been proposed to be sufficient for correction of LQT2 mutations (Rajamani *et al*. 2002). To analyze the effects these compounds have on $K_v11.1$ functionality and kinetics, whole cell patch clamp technique is used to study various

expressions of hERG. This electrophysiological technique permits intracellular access and recording of ionic currents arising from all ion channels at the cell surface. The properties of hERG PAS domain mutants will be assessed following overnight drug treatment, required to increase cell surface hERG expression. Utilizing protocols previously used to characterize $K_v11.1$ kinetics and functional channel quantification (Vandenberg *et al*. 2012; see *methods*), this study will determine whether candidate drugs that induce an increase in the cell surface expression of mutant hERG are associated with an increase of $K_v11.1$ current, and rescue of abnormal PAS domain mutant gating. The patch clamp technique will examine the properties of hERG PAS domain mutant gating.

Review of the Relevant Literature

Inherited LQT2

The congenital form of LQT2 is an inherited syndrome linked to an increased risk of cardiac arrhythmias and sudden cardiac death. By definition, this disorder is defined by an increased duration of the QT interval observed in the electrocardiogram (ECG). Cased by a loss or reduction of repolarizing currents, prolongation of the QT interval causes delayed repolarization of ventricular action potentials (Perry *et al*. 2015). In healthy individuals, the plateau phase of the cardiac action potential permits increased recovery of the rapid delayed rectifier current prevalent in cardiac muscle cells (I_{Kr}) from inactivation (Chiamvimonvat *et al.* 2017). Due to decreased rates of repolarization in ventricular myocytes, reduction in I_{Kr} is understood to be the major determinant of cardiac action potential duration.

Mutations in *KCHN2* (gene) lead to mutant variants of hERG (subunit) and thus $K_v11.1$. The congenital form of LQT2 is dominantly inherited with an approximate prevalence of 1:6000, and over 80% of missense mutations in the KCHN2 gene have been involved in LQT2 genotype-confirmed cases (Splawski *et al.* 2000; Anderson *et al.* 2006). The underlying causes for LQT2, based upon over 90% of known LQT mutants tested, are reduction of channel expression due to impaired release of mature hERG from the endoplasmic reticulum and accelerated protein degradation (Anderson *et al.* 2006, 2014; Ke *et al.* 2013). Other mechanisms, such as altered channel function have also been shown to result in LQT2 pathogenesis (Gong *et al.* 2011). Some mutant channels that display a reduction in protein trafficking also possess a gating defect (Ginaulus *et al.* 2011; Ke *et al*. 2013). Moreover, it has recently been shown that some hERG mutants may also be expressed at reduced cell surface levels due to cell surface instability

associated with rapid channel internalization and subsequent degradation (Apaja *et al.* 2013). None of the 500+ known hERG mutations linked to LQT2 is predominant (Schwartz *et al.* 2009). Nor do they possess "all-or-none" effects. They are graded and therefore variable amongst different mutants (Perry *et al.* 2015). Some mutations eliminate expression of mature hERG while others result in a milder phenotype (Ke *et al.* 2013). Over 30% of these LQT2 mutations may cause nonsense mutations, leading to a truncated, non-functional form of hERG mRNA that is immediately degraded (Gong *et al*. 2007). Although aberrant phenotypes of some mutants can be temperature rescued (Anderson *et al.* 2006, 2014; Ke *et al.* 2013), this is not a feasible clinical treatment. Suggested treatments target folding and trafficking pathways to restore WT phenotype from inherited mutations (Foo *et al.* 2015; Chianvimonvat *et al.* 2017).

Acquired LQT2

The $K_v11.1$ channel is the target of many (cardiovascular and non-cardiovascular) drug-induced arrhythmias, commonly referred to as acquired LQT2. Such drug-induced arrhythmias may be life-threatening due to QT prolongation and torsades de pointes (TdP) polymorphic ventricular tachycardia. Individual susceptibility depends on pharmacological risk factors and genetic predisposition. Structural heart disease and electrolyte imbalance may also contribute as potential risk factors (Foo *et al.* 2015; Chiamvimonvat *et at.* 2017; Grandi *et al.* 2017). In addition to the life-threatening arrhythmias caused by inherited LQT2, acquired LQT2 is equally lethal. Acquired LQT2 is often caused by direct blockade of $K_v11.1$ channels or disruption in hERG trafficking to the periphery (Sanguinetti *et al.* 2006; Yang *et al*. 2014). Consequently, before being made available for clinical use, all drugs must be tested in pre-clinical safety trials for potential effects on hERG and I_{Kr} (Roden, 2004; Waring *et al.* 2015).

Drugs

Pharmacochaperons represent a promising therapeutic strategy for the rescue of mature mutant hERG cell surface expression, in the hopes of rescuing reduced I_{Kr}, as seen in LQT2. Certain pharmacological compounds can affect hERG indirectly without binding to the channel (Wang *et al*. 2007; Guo *et al*. 2009), thus it may be possible for pharmacological rescue of acquired LQT2 through an additive effect; either through accelerated protein trafficking to the cell surface, increased protein production, or improved stability of the functional channel at the cell surface.

This study focuses on the following three compounds. These candidates originate from a preliminary study that presented identified compounds with the best potential for rescue (see *results*, *discussion*): artesunate, DCEBIO, and anagrelide

Artesunate – Artesunate is pharmacologically classified as an amebicide (agent destructive to amebae) and an antimalarial (agent used in treatment against malaria; NCBI artesunate). Artesunate is commonly used as the drug of choice for severe and complicated malaria (Li *et al.* 2010). When used in humans, nearly all the administered artesunate is rapidly hydrolyzed to its active metabolite dihydroartemisinin. The pharmacokinetics of the drug and its metabolism is patient-specific (HSDB), however a volunteer study identified the clearing of artesunate to dihydroartemisinin on the scale of minutes, with the half-life of dihydrosartemisinin being approximately 45 minutes (Ramzy *et al*. 1994). The mechanism of artesunate action is thought to involve a reduced haem or non-haem ferrous iron, creating oxygen centered radicals, as well as interaction with parasite proteins that convert peroxide to hydroperoxide (HSDB

Artesunic acid). Chemical and physical properties, pharmacology and biochemistry, and toxicity are all further characterized on PubChem (NCBI artesunate).

DCEBIO – DCEBIO is a known calcium-activated potassium channel (IK_{Ca} and SK_{Ca}) opener, meaning it is known to increase the probability of channel opening. This effect has been reported in smooth muscle cells (Morimura *et al.* 2006) and hippocampal pyramidal neurons (Pedarzani *et al*. 2005). Further, DCEBIO has also been implicated in stimulating chlorine secretion in the mouse jejenum via a cAMP/PKA-dependent manner as a secondary response to potassium release (Hamilton *et al.* 2006). These findings, along with others, support the use of this compound as a potential therapy for cystic fibrosis (CF) and chronic obstructive pulmonary disease (COPD). Mechanistically, this was thought to be possible by stimulating chlorine secretion via activation of hiK1 K^+ channels followed by the activation of an apical membrane chlorine conductance (Singh *et al*. 2001). However, studies implicating DCEBIO as a therapy for CF and COPD stopped around 2013 due to the lack of potency and DCEBIO never made it to clinical trials. Chemical and physical properties are readily available on PubChem (NCBI DCEBIO).

Anagrelide – Anagrelide is a well characterized platelet-reducing agent. It is known to act mechanistically as a phosphodiesterase 3 inhibitor leading to decreased megakaryocyte maturation and thus decreased platelet production. It is used in the treatment of thrombocythemia (FDA Pharm Classes anagrelide). When absorbed orally, anagrelide does not accumulate in the palsma after repeated administration (HSDB anagrelide). Anagrelide has passed Phase 1 clinical trials with no adverse side effects and is now in Phase 2. A study on anagrelide's effect on cardiac repolarization, particularly the QT interval, revealed no significant change in the QT

interval of healthy volunteers. However, when the QT interval was normalized for heart rate (QRcNi, individual correction and QTcF, Fridericia's correction) a small shortening of the QTc interval was observed. This effect was attributed to an increasing heart rate, rather than a direct effect on the QT interval (Troy *et al*. 2014). Based on the observations made in the following study, the conclusions made by Troy *et al*. may be debated (see *results* & *discussion*). Chemical and physical properties, pharmacology and biochemistry, and toxicity are all further characterized on PubChem (NCBI anagrelide).

The K_v11.1 Channel

Keating and colleagues first identified mutations in *KCNH2* as the underlying cause for chromosome 7-associated long QT syndrome (Curren *et al.*1995). Shortly afterwards, Sanguinetti et al. (1995) and Trudeau et al. (1995) reported that the K_v11.1 channels underlie the rapid component of the delayed rectified K^+ current, have a high selectivity for K^+ over Na^+, and showed that these channels were the targets for class III antiarrhythmic drugs (Sanguinett *et al.* 1995; Trudeau *et al.* 1995). Each hERG subunit is comprised of six transmembrane segments, labeled S1 through S6. The hERG voltage sensing domain is comprised of segments S1-S4, while S5-S6 (along with the intervening pore loop) contribute to the pore domain (Vandenberg *et al*. 2012; Diagram 1). The positively charged S4 domain has been shown to be the primary voltage sensor for channel opening; a common feature in voltage gated channels (Piper *et al.* 2005; Subbiah *et al* 2004; Zhang *et al*. 2004). hERG contains cytoplasmic NH_2- and COOH-terminal domains. The NH_2 terminus contains a Per-Arnt-Sim (PAS) domain, which will be further discussed in a later section (Morais Cabral *et al.* 1998). The COOH terminus contains a cyclic nucleotide binding domain (cNBD) that has been shown to interacts with the PAS domain

and regulate channel gating (Gustina *et al*. 2011; Warmke *et al.* 1998).

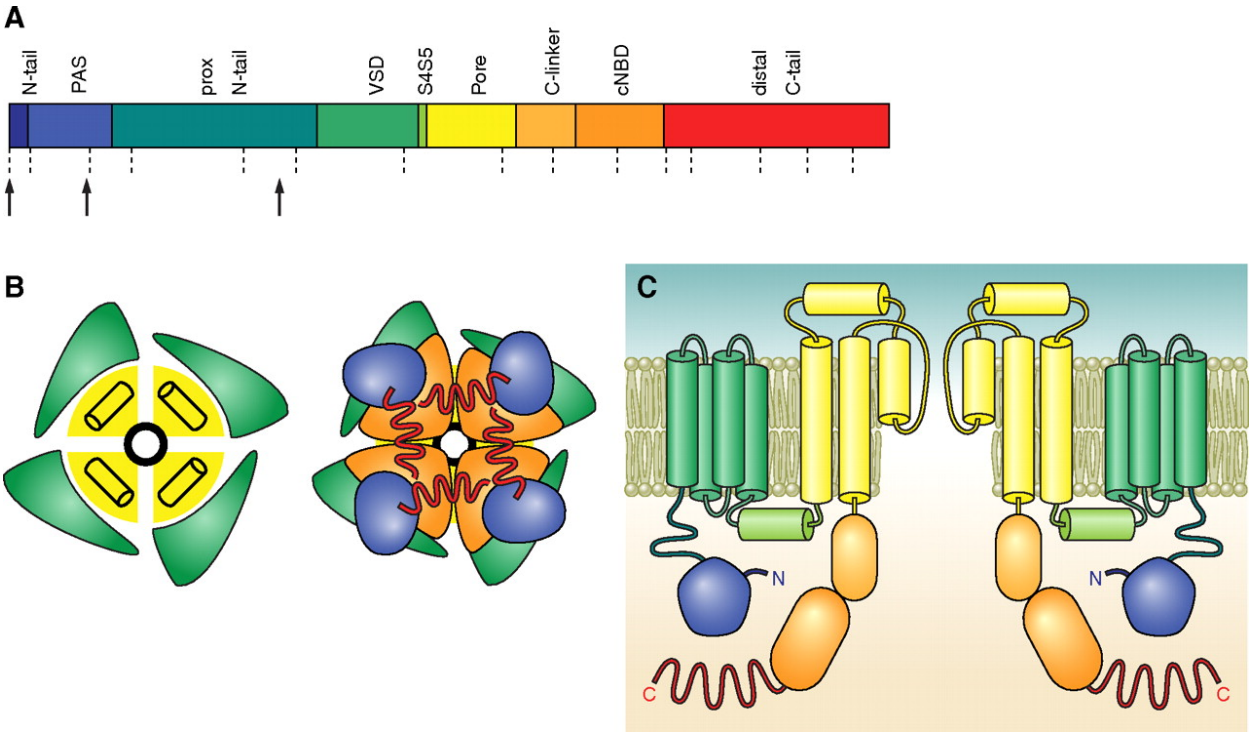

Diagram 1: Topology & structure of $K_v11.1$ channels (Vandenberg *et al*. 2012).

Functional $K_v11.1$ channels exist in the closed, open, or inactivated state; with unique gating that modulates their transition between each state. Channel inactivation has been shown to possess many unusual features, distinguishing the channels kinetics from other voltage gated K^+ channels. Namely, the kinetics of inactivation (channel transitioning from the open to the inactivated state) are much faster than the kinetics of activation (channel transitioning from the closed to open state; Schonerr *et al.* 1996; Smith *et al.* 1996; Spector *et al.* 1996). The inactivation process is voltage dependent (Sanguinetti *et al.* 1995). $K_v11.1$'s unique kinetics between gating states majorly contribute to its physiological role as the rapid component in cardiac repolarization.

The physiological role of $K_v11.1$ is best described in cardiac cells. These channels are the major determinant of the duration of the plateau phase of the cardiac action potential in both atrial and ventricular myocytes (Diagram 2). As mentioned, this is mainly a consequence of the channels slow activation and deactivation kinetics, coupled to the rapid, voltage-dependent inactivation and rapid recovery from inactivation (Sanguinetti *et al.* 2006; Smith *et al.* 1996). Proper maintenance of the duration of the plateau phase of the cardiac action potential is essential for proper calcium release from the sarcoplasmic reticulum, thus indirectly regulating cardiac contraction. This is ensured as $K_v11.1$ channels recover from inactivation as repolarization begins. By passing more inward current, $K_v11.1$ channels accelerate repolarization, leading to a greater recovery from inactivation. Together, this positive feedback loop ensures rapid repolarization. During the later portion of repolarization, I_{Kr} –conducting channels deactivate slowly and thereby remain open for a significant period after resting membrane potential has returned to resting/diastolic. Since the resting membrane potential of cardiac myocytes is approximately potassium equilibrium potential, the driving force is small and there is a little current flow through $K_v11.1$ channels in the early diastolic period (Vandenberg *et al*. 2012).

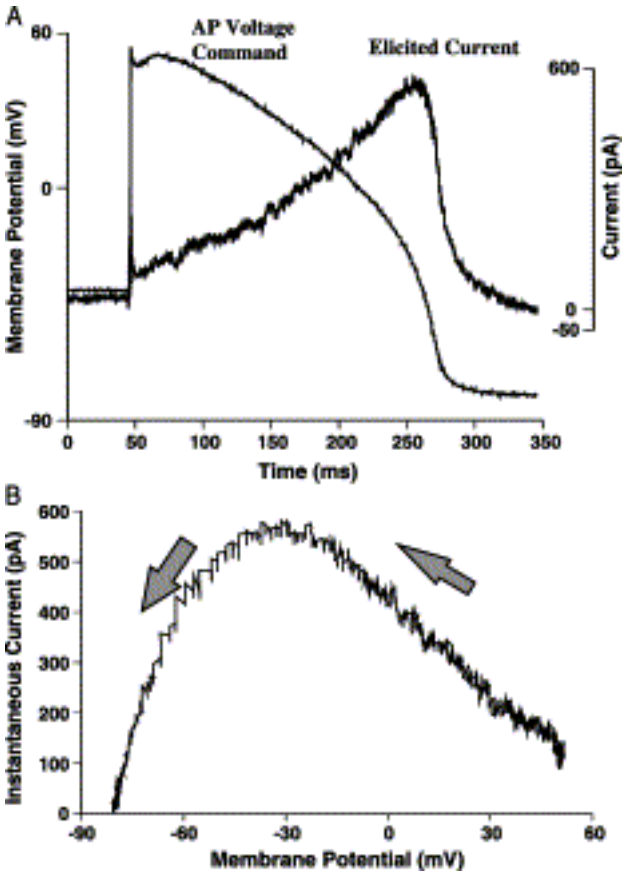

Diagram 2: Elicited hERG current during AP clamp showing how fast recovery from inactivation causes an increase in I_{Kr} current at the end of the platead of the cardiac AP. HERG cDNA was transiently transfected into CHO cells, and whole-cell patch clamp was performed. In panel A, the cell was stimulated by a voltage waveform derived from a rabbit ventricular cardiomyocyte (AP voltage command) and the elicited current measured. The current shown is a drug subtracted current. The holding potential was −40 mV to allow for direct comparison with similar currents measured in isolated myocytes in which the −40 mV potential was used to inactivate I_{Na}. In panel B, the instantaneous current–voltage relationship during AP repolarization (direction denoted by arrows) is plotted. Data, figure, and figure description acquired from Witchel *et al.*(2002).

Although we focus on K_v11.1 in the context of cardiac electrophysiology, the fully formed channels have been studied in other tissues and shown to be involved in spike frequency adaption and regulation of burst duration in neurons, regulation of resting membrane potential and action potential firing frequency in smooth muscle and endocrine cells. Further, hERG has been implicated in cell proliferation in tumor cells and schizophrenia (Vandenberg *et al*. 2012).

Channel Trafficking

Many mutations in the KCNH2 gene result in defects in protein biogenesis and trafficking (Sander *et al*. 2004). Improper protein biogenesis may occur at the level of mRNA processing (Zhang *et al.* 2004). mRNA stability (Gong *et al.* 2007), or protein folding and stability (Anderson *et al.* 2006; Ficker *et al.* 2003; Zhou *et al.* 1998). Since an underlying mechanism for LQT2 pathogenesis is thought to exist post-endoplasmic reticulum modifications, K_v11.1 trafficking will be highlighted from the endoplasmic reticulum to the cell (Foo *et al*. 2015).

HERG is expressed as two isoforms, hERG1a and hERG1b, which can form both homomeric and heteromeric ion channels. The first, hERG1a, consists of the full-length channel, which can be expressed at the cell surface as a tetrahomomeric functional channel that can independently pass current. The second, hERG 1b, possesses a short 35-residue N-terminal cytosolic sequence instead of a far more extensive cytosolic N-terminus (that includes the highly conserved PAS domain) found in hERG 1a (Phartiyal *et al.* 2008). Further, without co-expression of hERG1a, hERG1b cannot effectively traffic to the cell surface, but is delayed at the endoplasmic reticulum. Consequently, most studies of hERG in cellular systems analyze exogenous overexpression of hERG1a (Foo *et al.* 2015).

The journey of K_v11.1 from the endoplasmic reticulum to the plasma membrane is typical of other polytypic plasma membrane proteins. Newly synthesized hERG undergo N-terminal core glycosylation at the endoplasmic reticulum (Foo *et al* .2015). Core-glycosylated channels are then trafficked forwards to the Golgi apparatus, where the channels are "fully" glycosylated before final export the cell surface (Zhou *et al.* 1998; Petrecca *et al.* 1999; Gong *et al.* 2002). Once at the plasma membrane, mature K_v11.1 channels cycle between the plasma membrane and various endocytic compartments (Apaja *et al.* 2013; Foo *et al.* 2015).

As K_v11.1 matures and traffics to the cell periphery, channels experience multiple stages of regulation. At the endoplasmic reticulum, studies have revealed at least two distinct mechanisms of quality control: a HSP70/90 chaperone system that assists K_v11.1 folding (Peterson *et al*. 2012) and an endoplasmic reticulum associated proteasomal degradation system for degradation of misfolded proteins (Foo *et al.* 2015; Hantouche *et al.* 2016). Further, many distinct mechanisms are involved in channel regulation at the periphery. For instance, misfolded hERG channels have been shown to be targeted for degradation through channel ubiquitination (Apaja *et al.* 2013). Also, studies have shown that channel internalization and recycling can be both clathrin-dependent and –independent (Guo *et al.* 2012; Piper *et al.* 2014), along with unique pathways for endosomal sorting for lysosomal delivery (Sun *et al.* 2011; Apaja *et al*. 2013; Foo *et al.* 2015). Foo and colleagues have proposed that quality control occurs at the level of and both the endoplasmic reticulum and cell periphery contribute to LQT2 pathogenesis (Foo *et al.* 2015).

PAS domain

The hERG subunit possesses a Per-Arnt-Sim (PAS) domain at the cytoplasmic NH_2-terminal domain (Morais Cabral *et al.* 1998). The PAS domain has been a particular target of interest as it is a popular region for LQT2-causing mutations. For example, point mutations F29L, I31S, I42N, Y43C, and M124R, all located within a hydrophobic patch of the PAS domain result in reduced thermal stability and channel retention at the endoplasmic reticulum. This is presented as virtually no protein is expressed at the plasma membrane (Gianulis *et al.* 2011; Harley *et al.* 2012; Ke *et al* 2013). Assembled PAS domain mutants that do reach the periphery are known to display accelerated kinetics of channel deactivation (Chen *et al.* 1999). Subsequent studies identified that the altered gating was due to the disruption of the interaction between an amphipathic helix, located at the N-terminal tail and the hydrophobic patch on the PAS domain that helps stabilize the protein (Ng *et al.* 2011; Adaixo *et al.* 2013). These mutations also allow the endoplasmic reticulum quality control systems to target these misfolded proteins for degradation. Similar alterations in deactivation kinetics were observed in channels expressing point mutations in the cyclic nucleotide-binding domain (cNBD; Al-Owais *et al.* 2009). It was confirmed using various deletion mutants and florescence resonance energy transfer (FRET) spectroscopy that the N- and C- terminals interact to mediate channel gating in full length channels (Miranda *et al.* 2008; Gustina *et al.* 2011). Studies have shown that altered channel gating found in several PAS domain mutants could be rescued by a genetically encoded plasmid containing the PAS domain (Gianulis *et al.* 2011). Thermodynamic mutant cycle analysis identified several interactions between cytoplasmic domains which regulate the slow deactivation of $K_v11.1$. This study suggested that the loss of the energetically coupled Arg56 in

the PAS domain and Asp803 in the cNBD is likely what contributes to the fast deactivation kinetics observed in hERG PAS domain mutant R56Q (Ng *et al*. 2014). Other studies have shown that mutations in the PAS domain result in LQT2 because of reduced channel trafficking (Paulussen *et al.* 2002). This was later substantiated by studies which showed that PAS domain LQT2 mutants associated with altered domain-domain interactions reduced protein stability and channel trafficking (Harley *et al.* 2012; Ke *et al.* 2013).

The current study focuses on three PAS domain mutants: R56Q, M124R, and C64Y. Each mutant was selected as a representative of a sub-population of PAS domain mutants. R56Q was selected as a severe gating mutant, showing very rapid deactivation kinetics (Chen *et al.*1999; Ke *et al.* 2013). It's thermal stability and fully-glycosylated protein levels (western blot) are similar to WT (Ke *et al.* 2013), thus this mutant was selected to study if a drug candidate could rescue altered channel gating of PAS domain mutants. M124R was selected as a severe trafficking mutant. Although this mutant is known to have defects in deactivation, it was the protein's low thermal stability and fully glycosylated protein levels (Ke *et al.* 2013) that made M124R an excellent selection for studying the rescue of protein trafficking. Lastly, C64Y was chosen as a less severe trafficking and deactivation gating mutant. With thermal stability, fully glycosylated protein levels, and fast channel kinetics lower than WT (Ke *et al.* 2013), C64Y was selected to study if a drug could rescue a less severe defect in channel gating and/or trafficking.

Pharmacology of K_v11.1 Channels

Since the K_v11.1 channel is the target of a wide range of compounds that may lead to drug-induced arrhythmias (see *acquired LQT2*), pharmacological characterization of K_v11.1 has become a popular field. As a voltage gated ion channel, K_v11.1 undergoes many conformational

changes and is constantly in a dynamic state. Studies on how drugs bind $K_v11.1$ (ie. in what state, location, etc) has revealed minor differences in the mechanistic cause for channel block (Vandenberg *et al*. 2012). Armstrong published a series of papers which identified some of the first fundamental properties of K^+ channel block. Channel block from the intracellular side requires channel opening, and thus membrane depolarization; this can be observed by a decrease in K^+ current (Armstrong 1966, 1969, 1974). It was also shown that at hyperpolarizing potentials, below reversal for potassium, an inward flow of K^+ caused a dissociation of drug from the channel (Armstrong 1969, 1971, 1974). With this, a model was proposed that channel blockers acting from the intracellular side must pass through the channel pore to associate with the receptor site, and a narrowing of the channel gate prevent the drug from escaping (Armstrong 1971, 1974; Strichartz *et al*. 1973). Exceptions to this model are compounds that inhibit $K_v11.1$ trafficking and channel toxins (Vandenberg *et al.* 2012). Later Hille proposed that K^+ channel block can be described by the modulated receptor hypothesis, which suggests that drugs preferentially bind the inactivated state, rather than the open state (Hille 1977). More recent experiments using hERG mutants with impaired or removed inactivation changed the affinity of several drugs to the $K_v11.1$ channel (Ficker *et al*. 1998; Lees-Miller *et al*. 2000; Numaguchi *et al*. 2000; Yang *et al*. 2004). Today, it is accepted that preferential drug binding to $K_v11.1$ in the inactivated state is drug-dependent, and that some drugs have similar affinity for binding the open and inactivated states (Perrin *et al*. 2008).

Further, it has been shown that many compounds experience “drug trapping.” This term refers to the drugs that are retained in the channel pore during repolarization due to conformational change of $K_v11.1$ to the closed state. Smaller compounds are known to be more

easily trapped (Armstrong 1971). One of the major consequences of drug trapping is an accumulation of drug block with repeated depolarizations (ie. a train of action potentials), since drug dissociation between depolarizing steps is minimal. This phenomenon is referred to as "use-dependent block" and is commonly observed with local anesthetics and E4031, a specific hERG channel blocker (Courtney *et al*. 1975; Vandenberg *et al*. 2012). Compared to onset of K_v11.1 block, recovery from channel block is often relatively slow (Carmeliet 1992; Kamya *et al.* 2006; Mitcheson *et al*. 2000; Stork *et al.* 2007; Yang *et al*. 1995).

Besides reducing potassium conduction through the K_v11.1 pore, many compounds can reduce conductance of K_v11.1 via a "loss of function" mechanism associated with reduced channel trafficking to the periphery (Ficker *et al*. 2000; see *acquired LQT2*). This may be caused by alternative binding sites on the channel or off-target effects that regulate mature K_v11.1 trafficking (Ficker *et al.* 2003; Wang *et al*. 2009). Alternatively, some drugs have also revealed a "gain-of-function" phenomenon where upregulation of K_v11.1 channel trafficking is observed (Zhou *et al.* 2005; Stork *et al*. 2007), however, there are currently no known upregulators that do not block the channel pore (Perry *et al*. 2012; Sanguinetti *et al*. 2014). With this in mind, this study utilized the original ELISA based screen of a 5000 compound library identified 153 candidate hERG mutant correctors that were subsequently reduced to 56 candidates based upon the nature of the compound and potential feasibility as a therapeutic tool. Further evaluation as to potential binding to the consensus pore-binding site, reduced the list to 15 compounds. This study focuses on three of these compounds (artesunate, DCEBIO, and anagrelide) as potential non-blocking hERG correctors using an electrophysiological technique.

Methods - A

Plasmids and transfection

The hERG wt, F627Y and S641A expression constructs have been described previously (Walker et al., 2007; Walker et al., 2010, Apaja et al. 2013). PAS domain mutations were engineered using the Q5 site-directed mutagenesis kit (NEB, US) and inserted as a BstEII/HindIII fragment. All hERG constructs contain an HA-tag in the first extracellular loop which does not interfere with processing and function (Akhavan et al., 2003).

HeLa cells stably expressing wt and PAS-mutant hERG were generated by lentiviral transduction as described previously (Apaja et al 2013). Briefly, hERG coding sequence was shuttled into the pTZV4-CMV-IRES-puro plasmid (Open Biosystems) and packed into lentivirus using the Lenti-X HT Packaging System (Clontech, USA). Parental HeLa cells were transduced and a mixture of clones were selected using 1 μg/ml puromycin.

Transient transfection of HeLa cells was done using Genejuice (EMD milipore, USA) 48-72 h prior to analysis.

Cell-surface ELISA

hERG cell-surface expression and stability was measured using cell-surface ELISA as described previously (Apaja et al. 2010, Apaja et al. 2013). Briefly, the engineered extracellular HA-epitope was sequentially labelled with mouse monoclonal anti-HA Ab (1:1000 dilution, Covance, Canada) and HRP-conjugated secondary F'ab (Amersham Biosciences, Canada). For cell-surface stability measurements, cells were chased for the indicated times at 37°C prior to secondary Ab binding. Bound HRP-conjugated F'ab was detected using SuperSignal™ West

Pico Chemiluminescent Substrate (ThermoFisher, US). Non-specific binding signal was determined using a non-specific IgG primary Ab instead of the anti-HA Ab.

High-throughput screening

hERG-expressing HeLa cells were seeded onto white-bottom 96w tissue culture plates (Greiner Bio-one, Germany) two days prior to cell-surface hERG measurement. Following overnight treatment at 2uM, PM-hERG expression was measured using cell-surface ELISA. Cell viability was determined using AlamarBlue viability indicator (ThermoFisher, US). Measurements were performed in triplicate and expressed as percent relative to vehicle control (DMSO) normalized for viability. Candidates resulting in upregulation 5x standard deviations above DMSO control were selected for further study.

Materials

Small molecule library was obtained from McMaster University HTS lab (McMaster University, Canada) and prepared as 2mM stock solutions in DMSO. This library is a combination of the Prestwick Chemical Library (539 compounds, Prestwick chemicals, France), BIOMOL^{2865} Natural Products Library (501 compounds, Enzo Life Sciences, US), Lopac^{1280} International (1240 compounds, Sigma-Aldrich, Canada) and Spectrum Collection (1641 compounds, MicroSource Discovery Systems, USA).

Methods - B

Tissue culture.

HeLa cells stably expressing hERG were thawed from liquid-nitrogen storage and cultured at 37 °C, 5% CO_2 in Dulbecco's modified Eagle's medium (DMEM, high glucose, Gibco). DMEM was supplemented with 10% fetal bovine serum (FBS, Wisent Inc), 1% penicillin-streptomycin (Wisent Inc), 500 μL of 1 μg/ml puromycin (Gibco) and stored at 4 °C. Cellular medium was changed every 72 hours. Cells were passaged every 2-4 days, and maintained for a maximum of 25 days in culture. Passaging was performed using 0.05% trypsin (Wisent Inc) after a singular cell-washing with 1x phosphate buffered saline (PBS, Gibco). Cells were trypsinized for a maximum of three minutes at 37 °C, 5% CO_2 before being split. Cells were split to a minimum of 20% confluency and grown in either 60- or 100mm-diameter Petri dishes.

Although both WT and mutant hERG have shown to be sensitive to trypsinization (Gong *et al* 2006) electrophysiological data analysis were controlled within the various populations and normalized to maximum current (see *electrophysiology*).

Cells stored in liquid nitrogen were prepared in a freezing media containing 70% pure DMEM, 10% DMSO and 20% FBS. They were initially slowly frozen at -80 °C and stored for 1-4 weeks prior to storage in liquid nitrogen.

Stable cell lines were created by viral transduction (Lenti-X kit, Clonetech) and selected using puromycin. Wild type (WT) hERG and PAS domain mutants R56Q, C64Y, and M124R plasmids contained an HA-tag in the first extracellular loop that does not interfere with processing and function (Akhavan *et* al. 2003) and were prepared by Brian Foo (PTZV4-IRES-

Puro) as previously described (Apaja *et. al.* 2013). RT-PCR conducted (*n*=3) by Brian Foo showed the following (written as "plasmid mean ± SEM") for quantification of mRNA levels of the respected plasmid: WT 1.09 ± 0.03, R56Q 1.05 ± 0.05, C64Y 2.40 ± 0.11, and M124R 1.68 ± 0.18.

Drug preparation.

Drugs were prepared and stored as indicated by the manufacturer. Drugs were aliquoted and dissolved to either 100 mM and 2 mM stock solutions in DMSO, and stored at -20 °C. Drugs were thawed at room temperature and vortexed for approximately 5 seconds before use.

Solutions.

Internal pipette solution contained 135 mM KCl, 5 mM EGTA, 1 mM $MgCl_2$, and 10 mM HEPES dissolved in ddH_2O (Table 1). pH of internal solution was adjusted to 7.2 with 1 M KOH. Osmolality was adjusted to approximately 278 mOsm.

Control external patch-clamp bath solution (external solution) contained 135 mM NaCl, 5mM KCl, 2 mM $CaCl_2$, 1 mM $MgCl_2$, and 10 mM HEPES dissolved in ddH_2O (Table1). External solution pH was adjusted to 7.4 with 1 M NaOH. Osmolality was adjusted to approximately 300 mOsm.

DCBEIO (TOCRIS) or anagrelide (TRC Canada) were added to the external patch-clamp solution at a concentration of 2 μM, with the internal pipette solution remaining unchanged. Drug concentrations were chosen based on working concentration of preliminary data collected by Brian Foo.

Electrophysiology.

Poly-l-lysine-coated dishes were prepared as follows: 0.01% poly-l-lysine (Sigma Life Sciences) was diluted in ddH_2O to 0.1g/mL and added to a sterile 30-mm tissue culture dish; sufficient solution was added to cover the surface of the dish (approximately 3 mL). Solution-filled dishes were then incubated at 37 °C for 1-24 hours as outlined by the poly-l-lysine distributors (BrainBits, Genlantis). Poly-l-lysine solution was removed and the dishes were wrapped with parafilm and then stored at 4 °C for up to a week.

Cells from a single 60-mm dish were split and platted onto multiple 30-mm poly-l-lysine-coated tissue culture dishes and incubated for three hours at 37 °C to allow for sufficient cellular adhesion. Plated cells were then placed in a 35-mm Quick Exchange Platform (Model QE-1, Warner Instrumnets, Hamden, CT) within an inverted microscope (Zeiss Axiovert 135) and perfused at a rate of 1-2 mL/min with external solution (see *Solutions*). Cells were observed using a 40x/0,60 Korr Ph2 long distance lens (Zeiss).

Patch pipettes were constructed using boroscilicate glass capillaries (Warner Instruments). Both ends of the glass capillaries were manually fire-polished with a bunsen burner and then pulled using a microprocessor-controlled, multistage micropipette puller (P97, Sutter Instruments). Newly pulled tips were fire polished (ALA Scientific: CPM-2).

Prior to submerging patch pipette tips in external bath solution, tips of pipettes with a resistance of 1.5-3 MΩ were immersed in internal solution (see *Solutions*) and then backfilled with internal solution. Air bubbles were removed manually by flicking pipettes.

Cells were recorded at room temperature (approximately 21 °C). Perfusion of extracellular solution was allotted for 10 minutes prior to experimental analysis to ensure complete replacement of cellular media with external solution.

Cells were recorded using the whole-cell patch clamp configuration, as this has been shown to be a common and efficient means for studying effects of compounds on hERG currents (Goineau *et al.* 2012). Patch clamp experiments were performed using a VE-2 Voltage Clamp (Alembic Instruments) amplifier in tandem with a VE-2 headstage (Alembic Instruments). During the perfusion of external solution, a 1-4 M KCl salt-bridge ground was inserted into the bath and connected to the headstage.

Data were obtained using pClamp 10.2 (Axon Instruments) and a Digidata 1322A digitizer (Axon Instruments). Data were sampled at 20 kHz and filtered at 3 kHz. *n* refers to the number of cells recorded. No more than two cells were recorded from the same dish. No more than six cells were obtained from a given experiment.

Electrode holder (Warner Instruments) and headstage were manipulated using the MC1000e Controller (SD Instruments). Pipettes were submerged in extracellular solution and pipette voltage offset was manually nulled. Cells were selected using visual observation. Selected cells were round cells, with an intact cellular membrane, contained no protrusions or extensions, as these cells have shown the most promise to survive harsh voltage protocols in the whole cell configuration. The microelectrode seal with the cell membrane was achieved using a +5 mV depolarizing pulse for 10 ms from a 0 mV holding potential at 10 ms intervals. After the pipette tip and the cellular membrane were in contact, suction was manually applied to the pipette using a 5 mL syringe until a gigaohm seal was achieved. Prior to breaking through the

cell membrane, and entering whole-cell configuration, electronic capacitance compensation was performed to neutralize the rapid charging transient due to the patch pipette, as indicated by the user manual (Alembic Instruments). Additional suction was then applied while applying a -10mV, 20 ms depolarizing pulse from a holding potential of -80mv at 20 ms intervals. Following rupture of the patch, the pipette intracellular solutions was dialyzed for a minimum of two minutes. A membrane capacitance test protocol was imposed to determine membrane capacitance, membrane resistance, and access resistance using the clampex software. Capacitance was determined using a single exponential fit and represents the area under the curve of the transient current in response to the test protocol (Axon Instruments). Series resistance was compensated using a protocol provided by Alembic Instruments. The cell was subjected to a -30 mV hyperpolarization for 30 ms from a holding potential of -60 mV at 50 ms intervals. Fine tuning of capacitance compensation was adjusted to ensure proper series resistance compensation. This amplifier can achieve unprecedented 100% series resistance compensation using the full-scale range of 20 Meg and a frequency-selective attenuator, as instructed by Alembic Instruments user manual and described by Sherman *et al.* 1999.

The liquid junction potential (LJP) between the external solution and internal pipette solution (1.5 mV) was corrected offline using the formula (Neher, 1992):

$$V_{\mathrm{membrane}} = V_{\mathrm{pipette}} - V_{\mathrm{LJP}} \quad \text{(Eq. 1)}$$

All recorded currents came from cells with an access resistance less than 10 MΩ, membrane capacitance between than 15 and 40 pF, and a membrane resistance greater than 850 MΩ. Capacitance of WT K_v11.1 cells are (expressed as mean ± S.E.M.) 30.28 ± 1.313 for control, 29.95 ± 1.520 for DCEBIO treated cells, 28.76 ± 1.708 for anagrelide treated cells and

29.80 ± 0.8387 for all three populations. There was no statistical difference between the three populations (ANOVA p=0.7738 >0.05).

Once whole-cell configuration was achieved and cells passed membrane test exclusion criteria, various voltage protocols were imposed (see *Voltage Protocols*, *Acute Treatment*, and *Overnight Treatment*).

For experiments studying WT hERG or hERG mutants R56Q and C64Y, cells with peak currents less than 300 pA were excluded, as these currents were too small to be accurately analyzed to obtain channel kinetics and were not a proper representation of the population. All hERG-containing currents recorded in the M124R population were used, as these cells were expected to have extremely low currents (see *PAS domain*). Cells with change in baseline current > 50 pA were excluded, as change in baseline would have a direct consequence on recorded datum.

Large quantities of noise were found in recorded currents. Since amplitude of noise was constant throughout every trace of a given cell, amplitude of noise was subtracted from all recorded currents using the equation:

$$I_{\text{true}} = I_{\text{recorded}} - A_{\text{noise}} \qquad \text{(Eq. 2)}$$

where I is current and A is amplitude. Additionally, offline leak subtraction was performed on all voltage protocols. Leak was assumed to be linear for the voltage range of -160 mV to +50 mV (Ng *et al.* 2011). Three points were used to fit the linear line for leak subtraction: 1) origin; 2) peak-tail current at +50 mV after a 4 second -60 mV pulse; 3) peak current at the end of a 4 second, -60 mV pulse from a holding potential of -80 mV. The latter two points were plotted

since at these test potentials, no current is expected from $K_v11.1$, and any current observed is therefore assumed to be leak. Leak subtraction was applied to the recorded data as follows:

$$I_{Kv11.1} = I_{recorded} - I_{leak} \quad \text{(Eq. 3)}$$

where I_{leak} was corrected for every test potential of every cell using the linearity assumption

Voltage protocols.

Steady-state activation & inward rectification – Cells at a holding potential of -80 mV were subjected to successive +10 mV incremental depolarizing pulses (P1 pulse) for 4 seconds from -60 mV to +70 mV and then at the end P1 stepping to -50 mV for 4.5 seconds (Sanguinetti *et al.* 1995; Smith *et al.* 1996; Fig 7 inset). From baseline, the depolarizing P1 pulse induces $K_v11.1$ channels at the cell surface to transition from the closed, to the open, to then the inactivated state (Smith *et al.* 1996; C→O→I; Diagram 3). The hyperpolarizing P2 pulse forces inactivated channels to transition to the open and then closed state (Trudeau *et al.* 1995; Smith *et al.* 1996; I→O→C; Diagram 3). Inward rectification was measured by plotting the current-voltage (I-V) relationship between peak current at the end of depolarizing P1 pulse and the measured P1 voltage. The duration of the P1 pulse was long enough to ensure that all channels to transition to the inactivated state. Steady-state activation was measured using peak tail current analysis (Sanguinetti *et al.* 1995; Smith *et al.* 1996). Peak tail current at the beginning of the +50 mV P2 pulse was plotted against the previous depolarizing P1 voltage, as channels transition rapidly from the inactivated to the open state, and then more slowly to the closed state. Both steady-state activation and bell-shaped inward rectification I-V relationships are plotted as current density and normalized current (see *Statistical Analysis*). Current density and normalized

I-V plots for isochronal activation are fit with the Boltzmann sigmoid equation (least-squares fit) by the following equation:

$$Y = \text{Bottom} + \frac{(\text{Top} - \text{Bottom})}{1 + e^{\frac{V_{50} - X}{\text{Slope}}}} \qquad \text{(Eq. 4)}$$

where X is membrane potential, and Y is conductance. The Boltzmann fit of steady-state activation of peak tail currents from the P2 pulse yields the $V_{0.5}$ of activation and the slope factor, which is an approximation for the activation gating charge (Tan *et al.* 2012; Vandenberg *et al.* 2012).

Rate of deactivation – From a holding potential of -80 mv, cells experienced a two-step voltage protocol to measure rates of deactivation. The first (P1) pulse depolarized the cells to +40 mV for 500 ms. During this pulse, cells transition from the closed, to the open, and then to the inactivated state (C→O→I). Cells were then subjected to -10 mV incremental hyperpolarizing steps for 2.2 seconds from -50 mV to -150 mV (P2 pulse). During this time, cells transitioned from the inactivated, to the open, and then to the closed state (Fig. 9 inset; Ng *et al.* 2011; Gustina *et al*. 2011; Vandenberg *et al*. 2012; I→O→C). Decay of tail current was fit from peak until the end of the P2 pulse with a bi-exponential (standard) Chebyshev fit (Trudeau *et al.* 1995; Ng *et al.* 2011) for every sweep. The Chebyshev fit is described by the equation:

$$f(t) = \sum_{i=0}^{n} A_i e^{\frac{-t}{\tau_i}} + C \qquad \text{(Eq. 5)}$$

where n refers to the number of exponential terms, t represents time (independent variable), and τ_I represents the time constant for i'th exponential. Time constants were extracted from bi-exponential fits, representing the rates of both slow and fast deactivation, and plotted against

their respective P2 voltage pulse. Duration of the P2 hyperpolarizing pulses were long enough to ensure the capture of both slow and fast channel deactivation. Pulse duration was decided to be set to three times the slowest time constant (Vandenberg *et* al. 2012).

Rate of inactivation – To accurately measure the rate of inactivation of $K_v11.1$, cells underwent a three-step voltage protocol. From a baseline of -90 mV, cells initially experienced a 500 ms, +40 mV (P1) pulse, forcing channels from the closed into the inactivated state (C→O→I). Cells were then hyperpolarized to -90 mV for 30 ms (P2) where channels transition from the inactivated to the open state (Kiehn *et al*. 1999; I→O)), followed by incremental depolarizing steps from -60 mV to +80 mV for 250 ms (P3; Smith *et al.* 1996) where channels transition from the open to the inactivated gating state (Fig. 11; O→I). Current decay during the P3 pulse (Fig. 11), from peak current to end of P3 pulse, was fit with a single exponential (standard) Chebyshev fit (Eq. 5, n=1). Time constants from single exponential fits were extracted and plotted against respective P3 voltage pulses to study rates of inactivation (Fig. 12; Vandenberg *et al*. 2012).

Rate of recovery from inactivation – Cells were subjected to a two-step voltage protocol from a baseline of -80 mV to measure rates of recovery from inactivation. Cells were initially depolarized with a 500 ms, +40 mV voltage pulse (P1) to force all channels at the cell surface into the inactivated state (C→O→I). Cells were then hyperpolarized with an incremental -10 mV pulse for 500 ms, from +40 mV to -160 mV (P2; Fig. 12 inset; Wang *et al.* 2010). Tail currents were fit with a bi-exponential (standard) Chebyshev function (Eq. 5, n=2) from the start of tail current of P2 pulse to the onset of plateau of the decaying slope (Vandenberg *et al*. 2012). Fitting excluded the transient associated with series resistance compensation. The fast time constant for

each sweep (depicting recovery from inactivation at upstroke) was plotted against P2 voltage pulse.

Steady-state inactivation – Steady-state inactivation was measured using the same two-step voltage protocol as described for *rate of recovery from inactivation*. Peak tail currents from P2 pulse were plotted against their respective P2 voltage (Wang *et al.* 2010). I-V plots were generated for both current density and normalized current (see *Statistical Analysis*).

Peak tail current analysis/Channel quantification correction – Channel quantification at the cell surface was estimated by peak tail current analysis using the following series of voltage steps: from a holding potential of -80 mV, cells were depolarized to +40 mV for 500 ms, and then hyperpolarized to -120 mV for 500 ms. A single exponential (standard) Chebyshev (Eq. 5, n=1) fit was applied from the peak of the tail current to the plateau of the decaying portion of the tail current, and then extrapolated back to the onset of the -120 mV pulse (Fig. 15C). Extrapolation was applied to correct for channel deactivation occurring from onset of hyperpolarizing pulse to peak of tail current (Sale *et al*. 2008). Corrected peak tail current was then plotted as a measurement quantification of $K_v11.1$ at the cell surface.

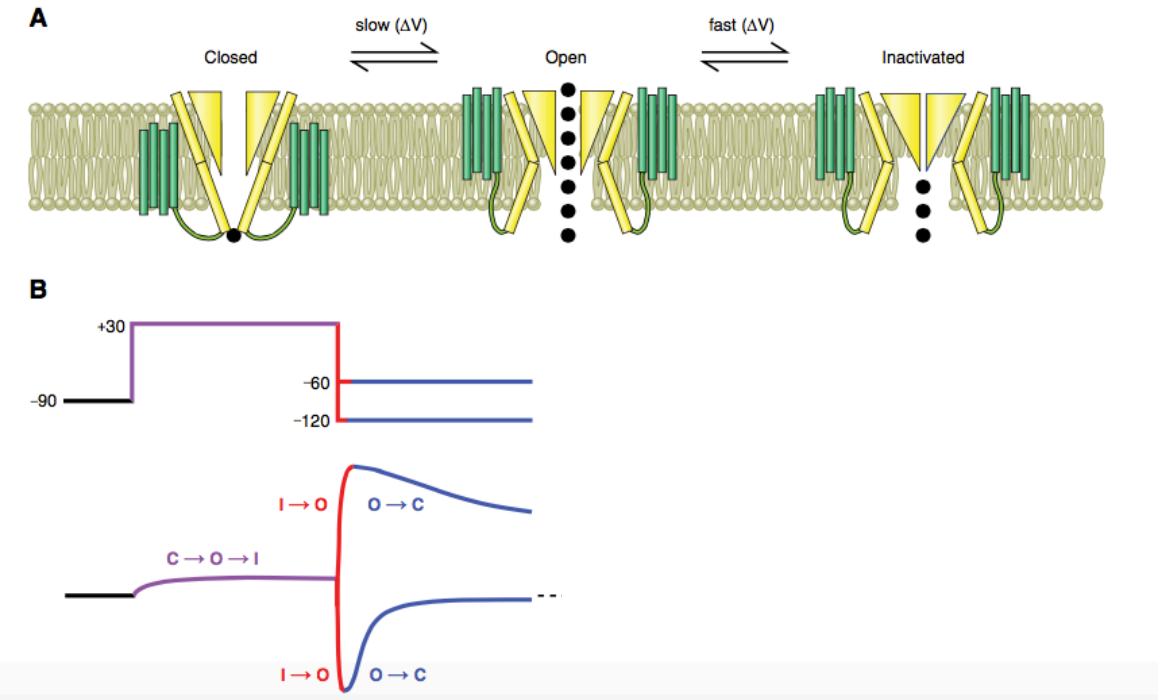

Diagram 3: Gating of K_v11.1 channels.
Kv11.1 channels can exist in closed, open, or inactivated states. Transitions between them are voltage dependent, with the transition between the closed and open states being slower than transitions between open and inactivated states (A). Redrawn current traces during the two-step voltage protocol shown at top of panel. Transitions between different states are color coded (B). Figure and figure legend extracted from Vandenberg *et al*. 2012.

Acute drug treatment.

WT hERG expressing cells were prepared and plated as outlined in *electrophysiology*. Cellular media was initially exchanged with untreated external solution (see *Solutions*). Once in whole cell configuration, the cell was stimulated with steady-state activation & isochronal activation voltage protocol (see *Voltage protocols*) to confirm and quantify cell-surface expression of functional WT K_v11.1. Perfusion of untreated external solution was then stopped and replaced with drug-containing external solution at 2 μM (see *Solution*; Table 1) at a constant rate of 1-2 mL/min. Perfusion was allotted for two minutes.

It has previously been shown that E4031 (negative control) blocks K_v11.1 in a use-dependent manner, such that the compound binds K_v11.1 as it transitions through its various gating states (Sanguinetti 1990; Ishii *et al.* 2003). To reduce the probability of false-positive "non-blockers," cells were stimulated repeatedly during the 10-15 minute perfusion period with a two-step voltage protocol (see *methodos*) to highlight compounds that may block K_v11.1 in a use-dependent manner. Repeat stimulation permits the additional benefit to qualitatively measure channel block (or washout) in real time. Cells were then repeatedly stimulated with a two-step voltage protocol starting from a holding potential of -80 mV (+20 mV depolarization for 4 seconds followed by a -50 mV hyperpolarizing pulse for 4.5 seconds) for 10-15 minutes to the monitor channel block in real time. Repeatedly stimulating cells with a +20 mV step and forcing K_v11.1 from the *closed* to *open*, to *inactivated* state ensures blockers that bind during gating transition will be properly screened. The cell was then stimulated with steady-state activation & isochronal activation voltage clamp protocol (acute treatment).

If the drug blocked the channel pore, drug-containing external solution perfusion was shut off, and replaced with a drug free external solution for 15 minutes to observe drug wash-out. The cell was then stimulated with steady-state activation & inward rectification voltage protocol to measure the effect of wash-out of drug on the blockade of K_v11.1 at the cell surface.

From the steady-state activation voltage protocol, peak tail current from P2 pulse of acutely treated cells was plotted as current density (pA/pF; see *Statistical Analysis*) and normalized against the current of the preceding P1 voltage pulse. Note: currents were normalized to the absolute maximal current of the initial drug free peak tail current recording (paired observation), opposed to peak tail current from drug containing solution recording. This provided

accurate measurement of channel block by the drug of interest. A maximum of one cell was recorded per acutely treated 30-mm dish.

Overnight drug treatment.

Overnight drug-treated cells (non-control) were prepared as outlined in *electrophysiology* with the following exceptions. Cellular media was exchanged for 2 μM drug-containing media, and incubated for 18-24 hours at 37 °C, 5% CO_2. Plating of cells on poly-l-lysine coated dishes on the day of experiment was conducted with 2 μM drug-containing media (oppose to untreated media). External solution used for perfusion in all overnight, drug treated experiments contained 2 μM of drug, in addition to the salts outlined in *solutions*. Internal solution remained untreated, as outlined in *solutions*.

Statistical analysis.

The total *n* for every experimental condition was obtained from a minimum of two separate inductions. All statistical analyses were performed using Graph Pad Prism 5.0. Data are expressed as mean ± S.E.M. unless noted otherwise. Current-voltage (I-V) plots are presented as currents normalized for cellular capacitance (picoampere/picofarad; pA/pF; see *Electrophysiology*). Normalized I-V plots are presented as I/I_{max} , where I_{max} is the maximum absolute current from the observed data. Sample traces shown are subject to a maximum of 200-fold data reduction. Statistical significance between groups greater than two were measured using one-way ANOVA. If statistical significance was observed, further analyses were performed. Differences in current were measured between two groups (generally experimental and control) using a one-way Student's *t*-test, unless otherwise indicated (see *Introduction* for evidence of one-way test). Differences in time constants (kinetics) were analyzed using one-way

ANOVA with Dunnett's Multiple Comparison Test post hoc. Data were considered significant when $p < 0.05$. Significant, precise p values are stated for ANOVA and t-test results. In post hoc t-tests, statistical significance is indicated as follows: *, $p \leq 0.05$; **, $p \leq 0.01$; ***, $p \leq 0.001$; ****, $p \leq 0.0001$.

External Solution	pH 7.4 (NaOH adjusted)	Internal Solution	pH 7.2 (KOH adjusted)
NaCl	135 mM	KCl	135 mM
KCl	5 mM	EGTA	5 mM
$CaCl_2$	2 mM	$MgCl_2$	1 mM
$MgCl_2$	1 mM	HEPES	10 mM
HEPES	10 mM		
Drug*	2 μM		

Table 1: Solutions for voltage clamp.
Recipe for external and internal solutions used in whole cell patch clamp experiments. See *methodology* for when drug was and was not used in external solution (*).

Results - Part A: Background screen of potential hERG correctors

Identification of potential hERG correctors

With the intention of identifying potential $K_v11.1$ downregulators, Brian Foo, a graduate student working under the supervision of Drs. Alvin Shrier and Gergely Lukacs, utilized the extracellularly HA-tagged WT hERG of stably expressing HeLa to conduct a cell surface ELISA assay. This screen evaluated the expression of cell surface hERG following overnight treatment of drugs from a 5,000 compound library (Fig. 1). BioActive compound library was obtained from McMaster University HTS lab and prepared as 2mM stock solutions in DMSO (Canadian Compound Collection: Prestwick, BIOMOL, Spectrum and LOPAC^{1280} subsets). Following 12-18 hour overnight drug treatment, cell surface $K_v11.1$ was detected using an anti-HA primary antibody and a horseradish peroxidase (HRP)-conjugated secondary antibody fragment, producing bioluminesce when exposed to ECL chemi-luminsecent substrate. Along with the identification of a number of $K_v11.1$ downregulators, 153 different compounds were observed to increase WT-hERG at the plasma membrane by a minimum of 5 standard deviations. The positive modulatory effect of these 153 drugs provides the potential that one or more of these compounds may correct certain hERG trafficking defects.

Further analysis and selection criteria narrowed the 153 potential channel upregulators to a pool of 57 drug candidates. Factors influencing the selection process included removal of compounds with a weak effect (<15% channel upregulation), non-FDA approved drugs (obsolete drugs, natural/endogenous products, industrial compounds, and poisons), topical compounds, chemotherapy agents (high probability of non-specific effect), and non-specific channel blockers.

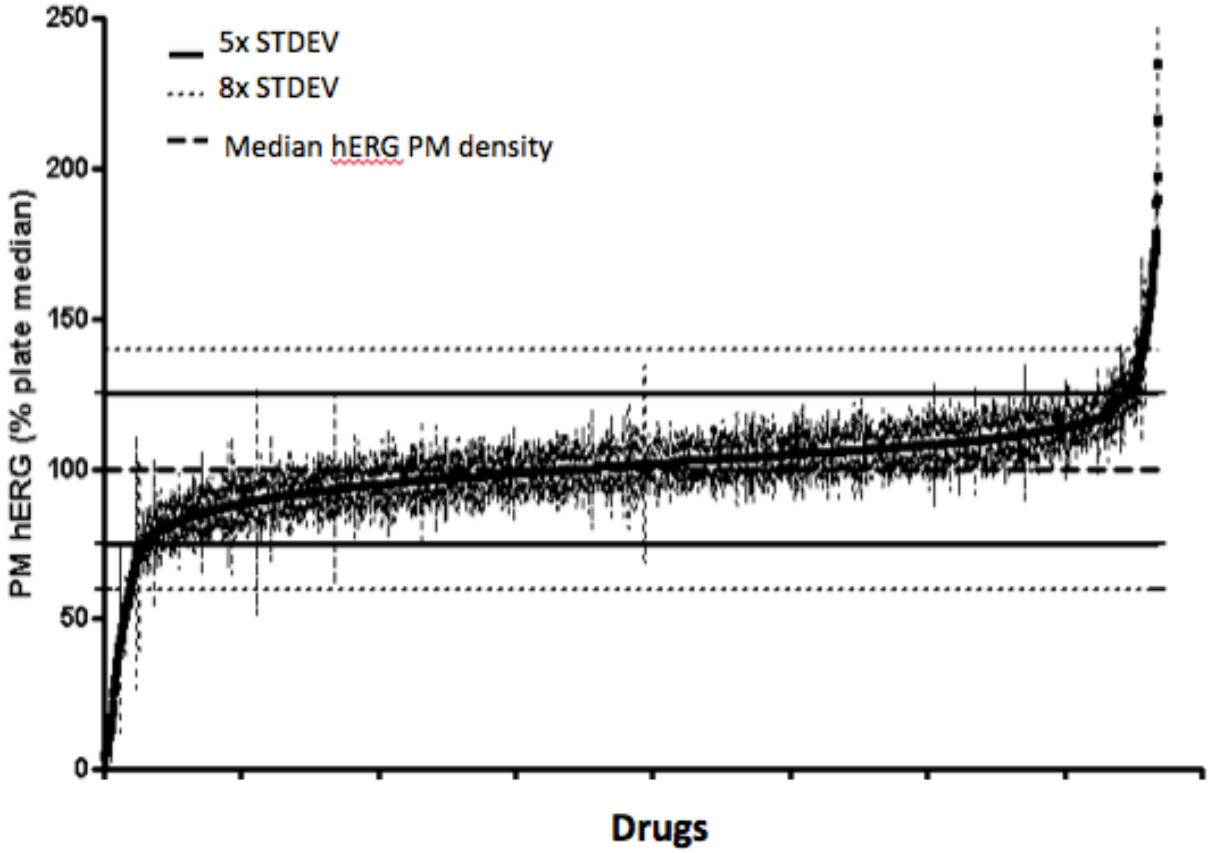

Figure 1: High-throughput drug screen
Quantification results of cell surface WT $K_v11.1$ expression by cell surface ELISA against extracellular HA tag following overnight (24 hour) drug treatment. Each horizontal point represents a different experimental condition (drug). 153 different compounds were classified as "upregulators" as they expressed more than 5x standard deviation. Datum is presented as plasma membrane expression of hERG as a percentage of control plate median. Dotted line represents 8x standard deviation. Solid line represents 8x standard deviation. Dashed line represents median hERG plasma membrane density. Error bars represent standard deviation of measurement performed in triplicated. All data were collected and analyzed by Brian Foo.

In addition to the identification of $K_v11.1$ upregulators, Brian Foo further analyzed the likelihood for some of these drugs to block the $K_v11.1$ channel pore. Methanesulfonailide class III antiarrhythmaic drug E4031 is known to both upregulate $K_v11.1$ expression and block channel pore (Sanguinetti *et al.* 1990; Sanguinetti *et al.* 1995; Zhou *et al*. 1999). It has also previously been shown that hERG channel blockers often bind the channel at the inner cavity, thus directly interacting with one, or both of the S6 aromatic residues Y652 and/or F656 (Sanguinetti & Tristani-Firouzi 2006). Hence, E4031, a well-characterized channel blocker and upregulator, was used as a control for studying channel block of the identified hERG upregulators. Mutations to Phe-656 (F656) have been previously shown to abolish both channel block and upregulation by known pharmacohaperones (Sanguinetti & Tristani-Firouzi 2006) for E4031. To investigate whether any of the compounds of interest block the channel pore at the S6 domain, population HeLa stably expressing WT hERG with a point mutation at residue Phe-656 (F656) for alanainie (F656A) was studied alongside WT (non-mutated; control). Cell surface ELISA experiment revealed upregulation of plasma membrane WT $K_v11.1$ when treated overnight with E4031 (2 μM), as expected (Fig. 2). When S6 F656 residue was point mutated to alanine, no upregulation was observed when treated overnight with E4031, as E4031 could no longer bind channel pore. Compounds revealing the same experimental outcomes as E4031 (control) for WT, and WT-F656A overnight treatment were suspected to block the hERG channel pore via inner cavity S6 binding. Compounds studied that showed no change in cell surface increase of WT hERG in the F656 point mutation condition were classified as non-hERG pore binding compounds at S6 domain, and thus unlikely to block the channel's pore. Cell surface ELISA experiment revealed that overnight treatment of compounds droperidol (7),

DCEBIO (9), danazol (10), AC-93253 iodide (11), zardaverine (26), and anagrelide (35) do not change the compounds modulatory effect in WT-F656A when compared to control. (control; Fig. 2; *n*=3), suggesting that these compounds upregulate hERG at the plasma membrane without binding pore segment S6 at residue F656. This further suggests that these compounds do not bind hERG at the channel's pore, and therefore unlikely to obstruct channel function. These five drugs were classified as potential non-blockers, with further analysis required.

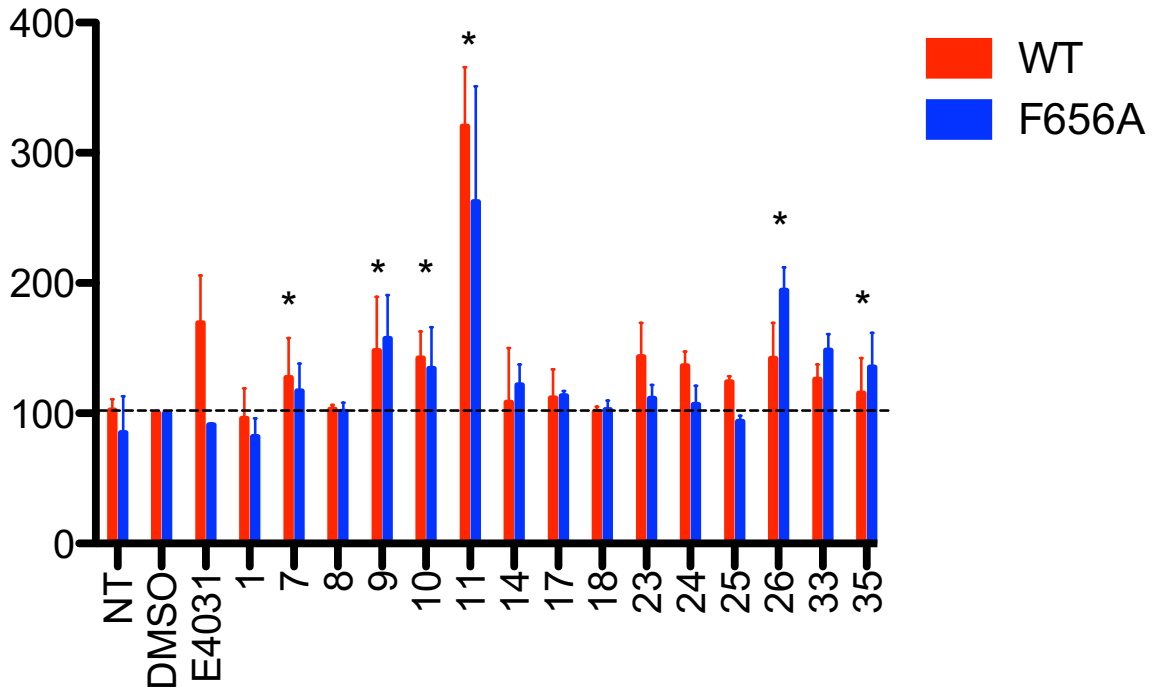

Figure 2: Indirect identification of K_v11.1 channel blockers
Quantification results of cell surface WT hERG (red), and WT hERG with Phe-F656 point mutation (F656A; blue) following overnight treatment of potential upregulator drugs at 2 μM (*n*=3). Daum is presented as plasma membrane expression of hERG as a percentage of untreated cells (control). Dashed black line indicated control (DMSO) plasma membrane expression. Asterix (*) highlights compounds that upregulated both WT and WT-F656A. Error bars represent standard deviation. All data were collected and analyzed by Brian Foo & Dr. Camille Barbier.

Drug-induced hERG upregulation in PAS domain mutants

To determine whether the potential $K_v11.1$ upregulators found in the high-throughput screen would in fact be useful clinically, the effect of the 57 drug candidates on various hERG PAS domain mutants (I42, I96, M124, R56, T65, and G601S) and WT (control) was measured using indirect cell surface ELISA technique. Experiments were conducted by Brian Foo and Michael Liben. It has previously been shown that most LQT2 mutations are caused by a trafficking-deficient mechanism (Anderson *et al*. 2006). Further, it has also been determined that mutations in the PAS domain of $K_v11.1$ channels cause a phenotypic trafficking defect (Ke *et al.* 2013). It was thus assumed that drugs that could rescue WT expression levels of one, or multiple, PAS domain mutants would be ideal candidates to treat LQT2.

Indirect cell surface ELISA experiments (n=1-3, where here n represents experiments, each done in triplicate) revealed two classes of the drugs: PAS specific rescuers and broad rescuers. Drugs were classified as "PAS specific rescuers" if cell surface ELISA showed upregulation for a minimum of one PAS domain mutant and did not upregulate non-PAS domain mutant G601S. Drugs were classified as "broad rescuers" if cell surface ELISA showed upregulation for a minimum of one PAS domain mutant, in addition to upregulation of non-PAS domain mutant G601S. Criteria for "upregulation" in cell surface ELISA experiments was defined as an increase of at least 15% mean expression of cell surface hERG following overnight treatment of relative to vehicle control (DMSO). Raw data were extracted and presented in a heat map as % of DMSO control (Fig. 3), to measure the strength of the upregulatory effect and % of WT (data not shown), measuring a given compounds potential to rescue normal levels of hERG at the plasma membrane. Of the 57 drugs further analyzed in the various hERG mutants, 13 were

classified as PAS-specific rescuers and 38 were classified as broad rescuers. The upregulation observed in the high throughput screen for WT hERG (Fig. 1) could not be replicated in any of the mutants (PAS and G601S) for eight of the compounds. All six compounds previously identified as non-pore blocking candidates (Fig. 2; droperidol, DCEBIO, danazol, AC-93253 iodide, zardaverine and anagrelide) were classified as broad rescuers.

	WT	C64	T65	M124
E4031	122	198	284	257
1	120	129	137	143
2	114	129	116	136
3	143	128	115	132
4	353	378	601	608
5	73	81	97	68
6	95	105	124	117
7	120	136	161	176
8	126	131	158	153
9	201	194	215	277
10	147	137	145	164
11	267	324	559	487
12	101	98	107	108
13	94	93	97	86
14	136	155	155	197
15	223	312	330	379
16	125	139	159	142
17	120	146	155	167
18	130	149	148	147
19	107	124	122	131
20	94	96	117	95
21	85	86	109	86
22	242	227	328	330
23	107	166	219	229
24	153	213	267	310
25	148	196	244	303
26	179	186	217	230
27	111	114	123	100
28	92	85	101	85
29	210	153	230	196
30	99	114	158	136
31	99	115	117	121
32	106	119	127	131
33	123	152	193	201
34	100	113	122	99
35	148	124	149	156
36	91	91	103	81
37	79	63	101	78
38	82	96	112	85
39	104	118	128	107
40	107	131	164	153
41	119	138	150	139
42	110	118	125	105
43	97	95	106	96
44	95	84	113	80
45	74	70	103	69
46	85	77	100	79
47	82	94	126	95
48	83	89	105	86
49	115	99	120	110
50	102	94	109	88
51	93	95	115	103
52	77	63	88	66
53	67	60	101	60
54	63	61	85	48
55	86	80	107	64
56	87	91	110	77
57	88	118	167	123

Scale (% control)

70
80
90
100
110
120
130
140
150
160
170
180
190
200
210
220
230
240
250
260
270
280
290
300

Figure 3: Steady-state expression of $K_v11.1$ relative to control.
Heat map of cell surface expression via indirect cell surface ELISA assay following drug treatment on WT and PAS domain mutants (C64, M124, T65). NT represents no treatment; DMSO is the vehicle control; E4031 is the positive control. Data is presented as relative percentage difference from vehicle control. (*n*=3). The scale represents signal amplitude as defined by relative intensity. All data was collected and analyzed by Brian Foo & Michael Liben.

Data for all 57 drugs is summarized in a heat map (Fig. 3), however data for the following artesunate, DCBIEO and anagrelide are highlighted. Artesunate (1) was classified as a PAS specific rescuer, with no significant upregulation of WT K_v11.1 when compared to DMSO (vehicle control; 100 ± 16% S.D.; *n*=2). DCEBIO (9) was classified as a broad rescuer with an upregulation of cell surface K_v11.1 expression in WT (144 ± 20% S.D.; *n*=2), R56Q (144 ± 8% S.D.; *n*=1; data not shown), M124R (147 ± 16% S.D.; *n*=2), and G601S (264 ± 37% S.D.; *n*=2; data not shown) when normalized to DMSO-treated cell surface expression (vehicle control). Anagrelide (35) was classified as a broad rescuer with an increase of cell surface K_v11.1 expression in WT (134 ± 13% S.D.; *n*=2), R56Q (171 ± 10% S.D. *n*=1), M124R (127 ± 6% S.D.; *n*=1), and G601S (238 ± 42% S.D.; *n*=2) when normalized to DMSO-treated cell surface expression. This data suggests that DCEBIO and anagrelide have the potential to upregulate hERG at the plasma membrane in a variety of hERG mutants, including significantly defective trafficking mutant M124R (KE *et al* 2013). This data also suggests that artesunate possesses the potential to exclusively rescue hERG PAS domain mutants, particularly severe trafficking mutant I42N (KE *et al*. 2013), as it did not show a significant modulatory effect on WT, nor on non-PAS mutant G601S (data not shown). Measurement of % of WT was normalized using mean expression for WT K_v11.1 (no treatment; NT) was 101.3 ± 9% S.D., which it too is normalized to DMSO.

Results - Part B: Patch clamp studies of putative hERG correctors

Drug block screen

To determine if the drugs previously classified as non-pore blockers by the point mutation made in S6 domain (F656A; Fig.2), electrophysiological studies using the whole cell patch clamp configuration were performed. This technique facilitates the analysis of acute drug treatment on channel functionality (ie. block or no block). Acute drug treatment was performed in WT hERG expressing cells as a means of confirming the assumptions made by the experiments conducted by Brian Foo. Acute block was studied with the following six compounds: artesunate (1), droperidol (7), DCEBIO (9), danazol (10), AC-93253 iodide (11), zardaverine (26), and anagrelide (35) (Fig. 3 & 4). Untreated cells were stimulated with the isochronal activation protocol (see *methods*) and used as a positive control (no block). Following identification of $K_v11.1$ currents, the cell was perfused with 2 μM drug-containing external solution. Solution was perfused for 10-15 minutes to ensure sufficient exchange of external solutions.

It has previously been shown that E4031 (negative control) blocks $K_v11.1$ in a use-dependent manner, such that the compound binds $K_v11.1$ as it transitions through its various gating states (Sanguinetti 1990; Ishii *et al.* 2003). To reduce the probability of false-positive "non-blockers," cells were stimulated repeatedly during the 10-15 minute perfusion period with a two-step voltage protocol (see *methodos*) to highlight compounds that may block $K_v11.1$ in a use-dependent manner. Repeat stimulation permits the additional benefit to qualitatively measure channel block (or washout) in real time.

Following drug perfusion, cells were again stimulated with iscohronal activation protocol. Peak tail currents were extracted and plotted as current density (Fig. 4) and normalized current (Fig. 5). The isochronal activation outlined in Methods section, was used to study the acute effects of each compound on hERG, since this voltage protocol provides an indirect measure of the number of channels at the cell surface. Due to the fast recovery of $K_v11.1$ from inactivation, relative to deactivation, the peak tail current observed in the -50 mV hyperpolarizing P2 pulse gives a relative indication of the number of channels activated in the previous depolarizing P1 pulse (Vandenberg *et al* 2012). Currents shown in Figure 5 are normalized to the tail current observed in the paired, no treatment observation, to best measure acute changes in the number of channels activated in the previous P1 pulse. Contrary to what is outlined in the Methods section, these I-V plots were not fitted with the Boltzmann function (Eq. 4), as this acute treatment study was done with sole intention of determining drug block.

Qualitative analysis of peak tail current recordings following acute drug treatment revealed that artesunate (Fig. 4A & 5A), DCEBIO (Fig. 4C & 5C), danazol (Fig. 4D & 5D), and anagrelide (Fig. 4F & 5F) do not block the $K_v11.1$ channel pore. Although it appears that these compounds cause a partial block, they were all classified as non-blockers. This was based on the expectation that there is a leak that cannot be corrected for when the paired treatment observation is made after over 10 minutes in the whole cell configuration. Acute drug treatment also revealed that droperidol (Fig. 4B & 5B; Stork *et al*. 2007) and AC-93253 iodide (Fig. 4E & 5E) do block the $K_v11.1$ channel pore; as currents showed no statistical difference from negative control (E4031; $p>0.05$). It has been previously shown that there exists a degree of variability of $K_v11.1$ channel block by known inhibitors at physiological temperatures when compared to studies made

at room temperature (Kirsch *et al*. 2004). These studies however, do not reveal that experiments conducted at room temperature led to any false-positive or -negative results, but highlights that the sensitivity of channel inhibition is temperature dependent. This indicates the experimental procedure outlined (see *methods*) is sound in its ability to determine whether a given drug does or does not block $K_v11.1$ conductance.

To determine if channel block caused by droperidol and AC-93253 iodide could be reversed, paired observations were perfused with untreated external solution to allow for drug washout. After washout, cells were stimulated with isochronal activation protocol to study if rescue of non-treated condition is possible. Following a 15-minute washout using untreated extracellular solution, neither drug was able to be washed out (data not shown). Replication of voltage-dependence of recovery from drug block for droperidol was not observed, as two-step voltage stimulation was not invoked during 15-minute washout (Stork *et al*. 2007). The same is true for AC-93253 iodide, however since this compound has not been previously characterized, it may also be classified as a "trapped" drug.

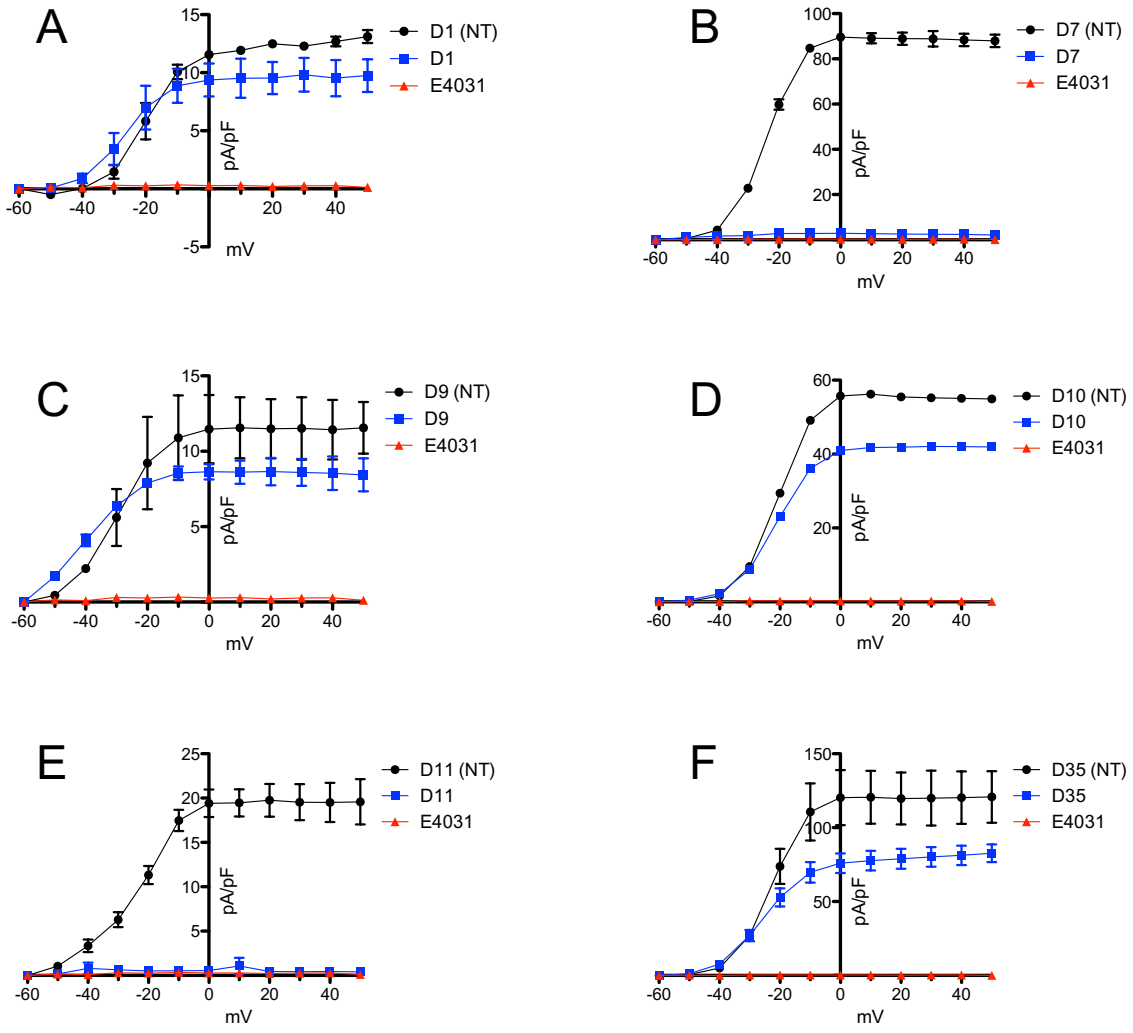

Figure 4: Acute drug treatment on WT $K_v11.1$ measured as current density.
Steady-state activation I-V curves for no treatment (positive control; black circles; *n*=1-3), paired observation following drug treatment at 2 μM (red squares) and un-paired E4031 treated cells (2 μM; negative control; black triangles; *n*=3). Acute treatment was performed for artesunate (A; *n*=2), droperidol (B; *n*=2), DCEBIO (C; *n*=2), danazol (D; *n*=1), AC-93253 iodide(E; *n*=2), and anagrelide (F; *n*=2). Peak tail currents at -50 mV following a series of depolarizing steps ranging from -60 mV to +50 mV were normalized to cell size (membrane capacitance; pF) and plotted against the previous depolarizing voltage pulse. Error bars represent S.E.M.

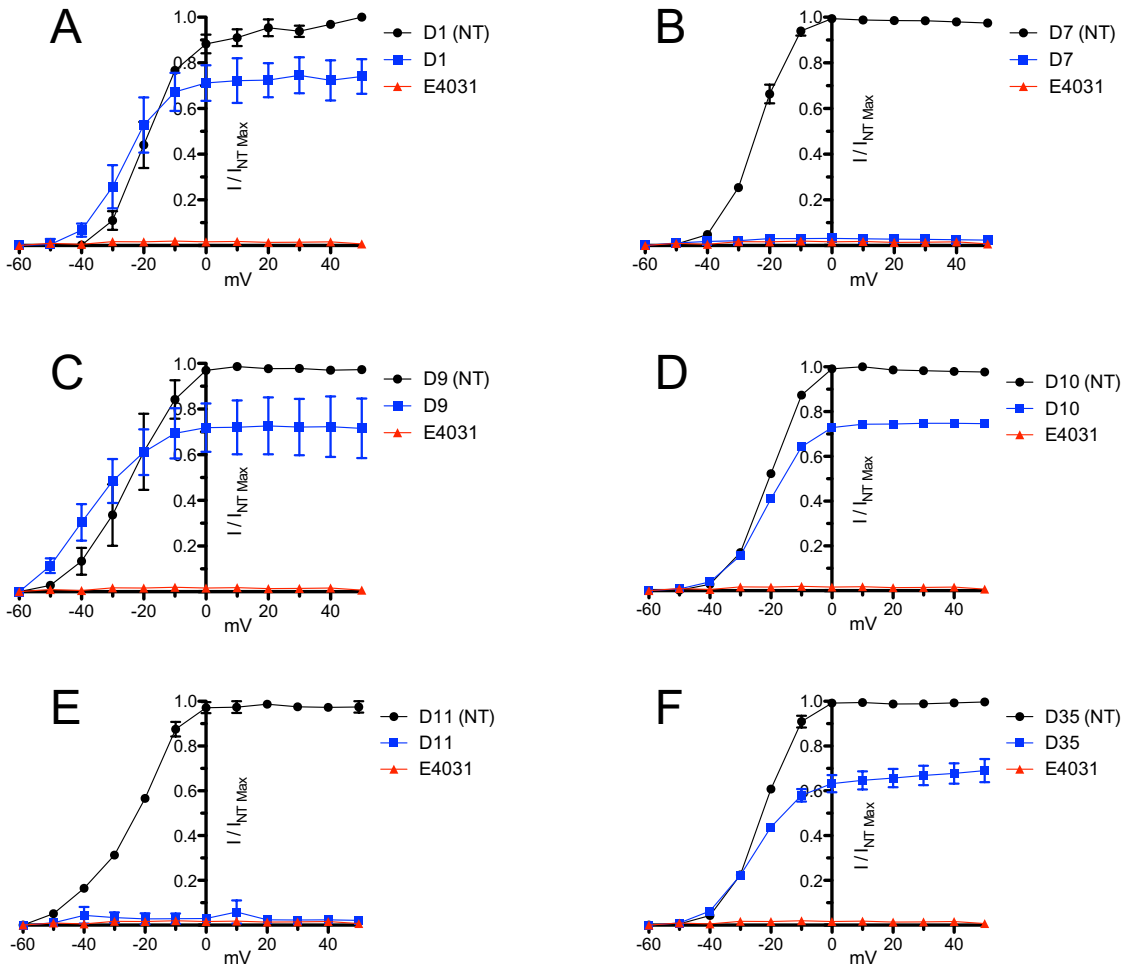

Figure 5: Acute drug treatment on WT $K_v11.1$ measured as normalized current. Normalized steady-state activation I-V curves for no treatment (positive control; black circles; *n*=1-3), paired observation following drug treatment at 2 μM (red squares), and un-paired E4031 treated cells (2 μM; negative control; black triangles; *n*=3). Acute treatment was performed for artesunate (A; *n*=2), droperidol (B; *n*=2), DCEBIO (C; *n*=2), danazol (D; *n*=1), AC-93253 iodide(E; *n*=2), and anagrelide (F; *n*=2). Peak tail currents at -50 mV following a series of depolarizing steps ranging from -60 mV to +50 mV were normalized to peak current from paired non-treated observation ($I_{NT\ Max}$) and plotted against the previous depolarizing voltage pulse. Error bars represent S.E.M.

Effects of artesunate on WT K_v11.1 expression

To measure if the upregulation observed in cell surface ELISA of WT K_v11.1 following treatment of artesunate (Fig. 2 & 3) could be replicated in channel functionality, WT K_v11.1 expressing cells were incubated overnight with artesunate and studied by patch clamp. Functional analysis was conducted using the two-step steady-state activation voltage protocol (Fig. 6C). From a holding potential of -80 mV, cells were subjected to +10 mV incremental depolarizing pulses (P1 pulse) for 7 seconds from -70 mV to +70 mV before stepping the voltage to -50 mV for 5 seconds. From the holding potential, the depolarizing P1 pulse induces channels to transition from the closed, to the open, and then to the inactivated state. The hyperpolarizing P2 is set to -50 mV to force the channels that were activated in the previous P1 pulse from the inactivated, to the open and then to end in the closed state (Sanguinetti *et al.* 1995; Trudeau *et al.* 1995). The rapid recovery of K_v11.1 from inactivation, relative to its slow deactivation properties permits use of the tail currents observed early in the P2 pulse as the functional quantification of hERG at the cell surface (Vandenberg *et al*. 2012). Although a more hyperpolarizing P2 pulse (i.e. -120 mV) would provide a more accurate measurement of functional channel quantification at the cells surface (see *methods*), a -50 mV pulse is sufficient to measure relative channel upregulation (i.e. overnight treatment vs. no treatment), as both experimental conditions experience the same voltage protocol, and thus the tail currents should reflect an equivalent proportion of the channels activated in the previous P1 pulse.

After being subjected to overnight treatment of artesunate at 2 μM (Fig. 6B), recorded currents were analyzed. I-V plots for bell shaped inward-rectification (Fig. 6 D&E) and steady-state activation (Fig. 6 F&G) were plotted as current density (Fig. 6 D&F) and normalized

current (Fig. 6 E&G). Current densities from the steady-state activation I-V (Fig. 6F) are, as previously described, a relative measure of channel quantification at the cell surface. Tail currents evoked following a P1 pulse to +60 mV were compared, as this voltage is sufficiently rightward along the Boltzmann curve to encapsulate maximal channel activation in the previous P1 pulse. Peak tail current for cells treated with artesunate was 125.52 ± 17.26 pA/pF, while that of NT cells was 46.14 ± 10.59 pA/pF. A one-tailed, unpaired *t*-test revealed that the mean peak tail-current of $K_v11.1$ is significantly greater in WT cells treated with artesunate than the no treatment WT control, $p = 0.0009$ (Fig. 6F). As this is a comparative measure, it can be shown that when cells were treated overnight with artesunate, cells exhibited approximately a 2.7-fold increase in peak tail current at -50 mV, following a P1 pulse to +60 mV. This suggests an equivalent 2.7-fold increase in WT $K_v11.1$ channels at the cell surface.

Steady-state activation I-V plots were fitted by the Boltzmann equation (Eq. 4; Fig. 6 F&G). Fitting normalized steady-state activation I-V plots with a Boltzmann curve provides additional kinetic analysis for changes in activation gating charge, measured by the slope factor, and half-maximal activation, measured by $V_{0.5}$. (Tan *et al.* 2012; Vandenberg *et al.* 2012). Slope factor for artesunate treated cells was 7.23 ± 0.69 units, compared to 6.61 ± 0.51 units for no treatment controls. $V_{0.5}$ of activation for artesunate treated cells was -22.48 ± 0.79 mV, compared to -22.59 ± 0.59 mV for no treatment controls. Additionally, administration of artesunate did not appear to shift the steady-state inwardly rectifying I-V curve (Fig. 6E). Together, these data demonstrate that artesunate upregulates cell-surface $K_v11.1$ current magnitude without altering channel kinetics; particularly it's activation properties. No further analysis of channel gating or kinetics were made for artesunate.

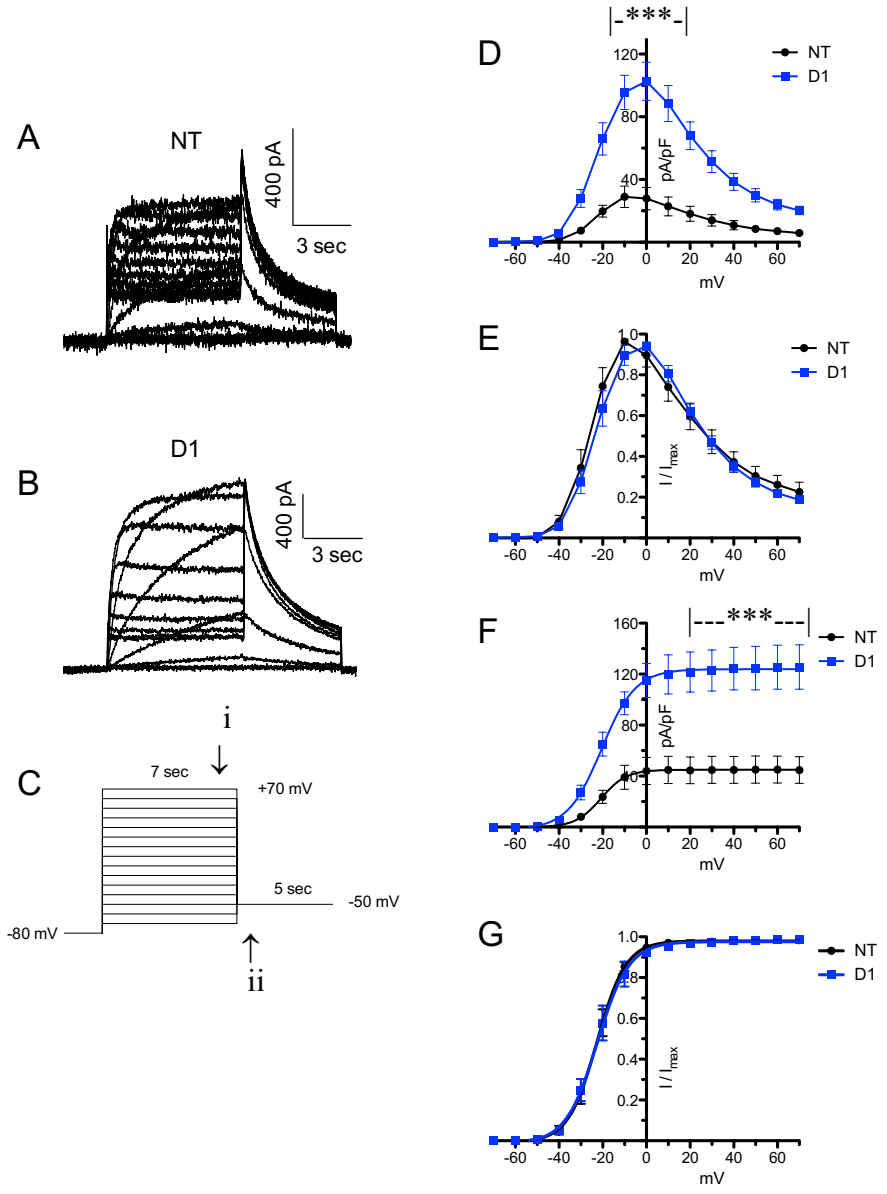

Figure 6: Artesunate-induced upregulation of WT $K_v11.1$

WT $K_v11.1$ expressing cells were treated overnight with artesunate at 2 μM. Cells were stimulated with a two-step voltage protocol: from a baseline of -80 mV, cells were depolarized in +10 mV incremental steps from -70 mV to +70 mV for 7 seconds (P1 pulse), and then hyperpolarized to -50 mV for 5 seconds (P2 pulse). Sample traces for no treatment (A; control), overnight treatment (B) are shown, along with voltage protocol (C). Bell shaped I-V curve showing inward rectification was plotted as current density (extracted at i; D) and normalized current (E). Steady-state activation I-V was as both current density (extracted at ii; F) and normalized current (G). NT represents no treatment (*n*=8) and D1 represents artesunate (*n*=10).

Effect of drugs on steady-state activation & inward rectification

To measure the effects of the drugs labelled as upregulators (Fig. 1), non-S6 domain-binding blockers (Fig. 2) and non-use-dependent blockers (Fig. 5) had on K_v11.1 functionality and kinetics, a preliminary analysis of steady-state activation was performed using the patch clamp technique. Two drugs are highlighted in this study: DCEBIO (9) and anagrelide (35). Both drugs were studied in cells stably expressing WT K_v11.1 and PAS domain mutants (R56Q, C64Y, and M124R). Cells were stimulated with a two-step voltage protocol following overnight treatment with the drug of interest. The protocol, slightly optimized from that used to study artesunate (Fig. 6C), has been summarized in *methods*, and is outlined in Figure 7 inset. From a baseline of -80 mV, cells were depolarized with a series of incremental +10 mV pulses ranging from -60 mV to +70 mV for 4 seconds, and then hyperpolarized to -50 mV for 4.5 seconds.

Steady-state activation I-V curves were plotted as current density (Fig.8 I-L) providing an approximate measure of functional channel quantification at the cell surface (Vandenberg *et al*. 2012), and normalized current (Fig. 8 M-P) providing approximate activation kinetics (Tan *et al.* 2012). Both I-V plots were fitted with the Boltzmann sigmoid function. Qualitative analysis of peak tail current measured at the P2 pulse, as seen in the current density steady-state activation I-V (Fig. 8 I-L), demonstrated a significant increase in functional K_v11.1 expression at the cell surface following treatment of both DCEBIO and anagrelide in WT (Fig. 8I), gating mutant R56Q (Fig. 8J), C64Y (Fig. 8K), and severe trafficking mutant M124R (Fig. 8L).

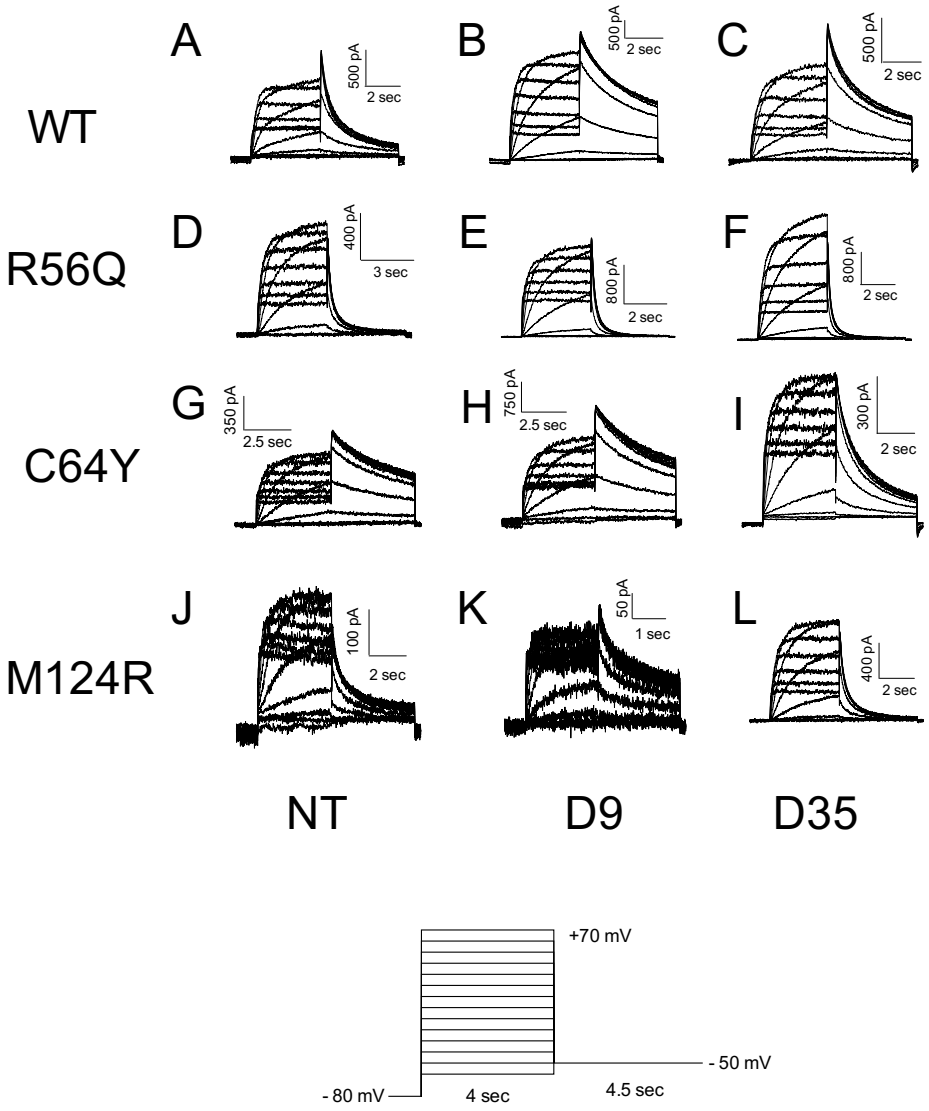

.

Figure 7: Drug-induced steady-state activation & inward rectification of $K_v11.1$.
Sample traces of $K_v11.1$ currents recorded from a two-step voltage protocol. Cells stably expressing WT (A-C), R56Q (D-F), C64Y (G-I) or M124R (J-L) were stimulated with a two-step voltage protocol. From a baseline of -80 mV, cells were depolarized in +10 mV incremental steps from -60 mV to +70 mV for 4 seconds (P1 pulse), and then hyperpolarized to -50 mV for 4.5 seconds (P2 pulse); inset. Cells were studied after overnight treatment of DCEBIO (D9; column 2), anagrelide (D35; column 3) or no treatment (NT; control; column 1). Data are reduced 200-fold.

To determine whether DCEBIO or anagrelide affected the activation kinetics of $K_v11.1$, slope factor and $V_{0.5}$ of the Boltzmann fit (Eq. 4) were studied. Normalized steady-state activation I-V plots (Fig. 8 M-P) were used as a more suitable comparative measure to account for variations amongst treatment conditions in current density magnitude. Slope factor, an approximation of the activation gating charge, for WT cells was 5.34 ± 0.59 units and 6.28 ± 0.33 units when treated with DCEBIO (*n*=8) and anagrelide (*n*=9), respectively. Slope factor for non-treated WT cells (*n*=12) was 7.54 ± 0.76 units. When compared to no treatment, a sum of squares F-test indicated that the slope factor for DCEBIO differed significantly ($F(1,232)=5.623$, $p=0.0185$), while that of anagrelide did not ($p>0.05$). This suggests that DCEBIO induces a decrease in activation gating charge on WT $K_v11.1$ and that the voltage dependence, as seen in the normalized steady-state activation I-V, is modified due to a decrease in voltage dependence of activation. Further, $V_{0.5}$ of normalized steady-state activation I-V plot was observed to be -22.90 ± 0.69 mV and -18.70 ± 0.35 mV for WT cells treated with DCEBIO and anagrelide, respectively. $V_{0.5}$ for non-treated, normalized WT currents was -25.55 ± 0.87 mV. A sum of squares F-test indicated that the $V_{0.5}$ for DCEBIO ($F(1,232)=5.417$, $p=0.0208$) and anagrelide ($F(1,244)=72.93$, $p<0.0001$) differed significantly when compared to that of no treatment control. This indicates that both drugs cause a rightward shift in WT currents, with a more severe shift caused by anagrelide. This rightward voltage shifts are also seen in bell-shaped inward-rectification I-V (Fig. E-H). Contrary to the observations made in WT, mutants R56Q, C64Y, and M124R exhibited no statistical difference in the slope factor, nor $V_{0.5}$ in their respective normalized steady-state activation I-V plots ($p>0.05$); suggesting that neither drug alters activation kinetics of hERG PAS domain mutants.

Together, analysis of steady-state activation following drug treatment suggests that qualitatively, DCEBIO and anagrelide upregulate functional $K_v11.1$ at the cell surface. DCEBIO causes a decrease in activation gating charge on WT. Both DCEBIO and anagrelide cause a rightward voltage shift in currents of WT. Neither drug modulates activation gating of PAS domain mutants.

hERG type + treatment	$V_{0.5}$ (mV)	Slope factor (k)
WT (NT)	-25.55 ± 0.87	7.54 ± 0.76
WT + D9	-22.90 ± 0.69	5.34 ± 0.59
WT + D35	-18.70 ± 0.35	6.28 ± 0.33
R56Q (NT)	-18.70 ± 0.35	6.05 ± 0.31
R56Q + D9	-19.60 ± 0.55	6.04 ± 0.49
R56Q + D35	-20.76 ± 0.46	6.13 ± 0.41
C64Y (NT)	-21.09 ± 0.92	7.10 ± 0.81
C64Y + D9	-25.05 ± 0.51	6.31 ± 0.44
C64Y + D35	-21.93 ± 1.65	8.62 ± 1.46

Table 2: Overview of drug induced $V_{0.5}$ and slope factors from in WT and hERG mutants. Half-maximal voltage of activation and slope factor measured from WT, R56Q, and C64Y expressing hERG measured using the Boltzmann fit. Fit was applied to normalized currents recorded from a two-step steady-state activation protocol (see *methods*). Data are presented as mean ± S.E.M.

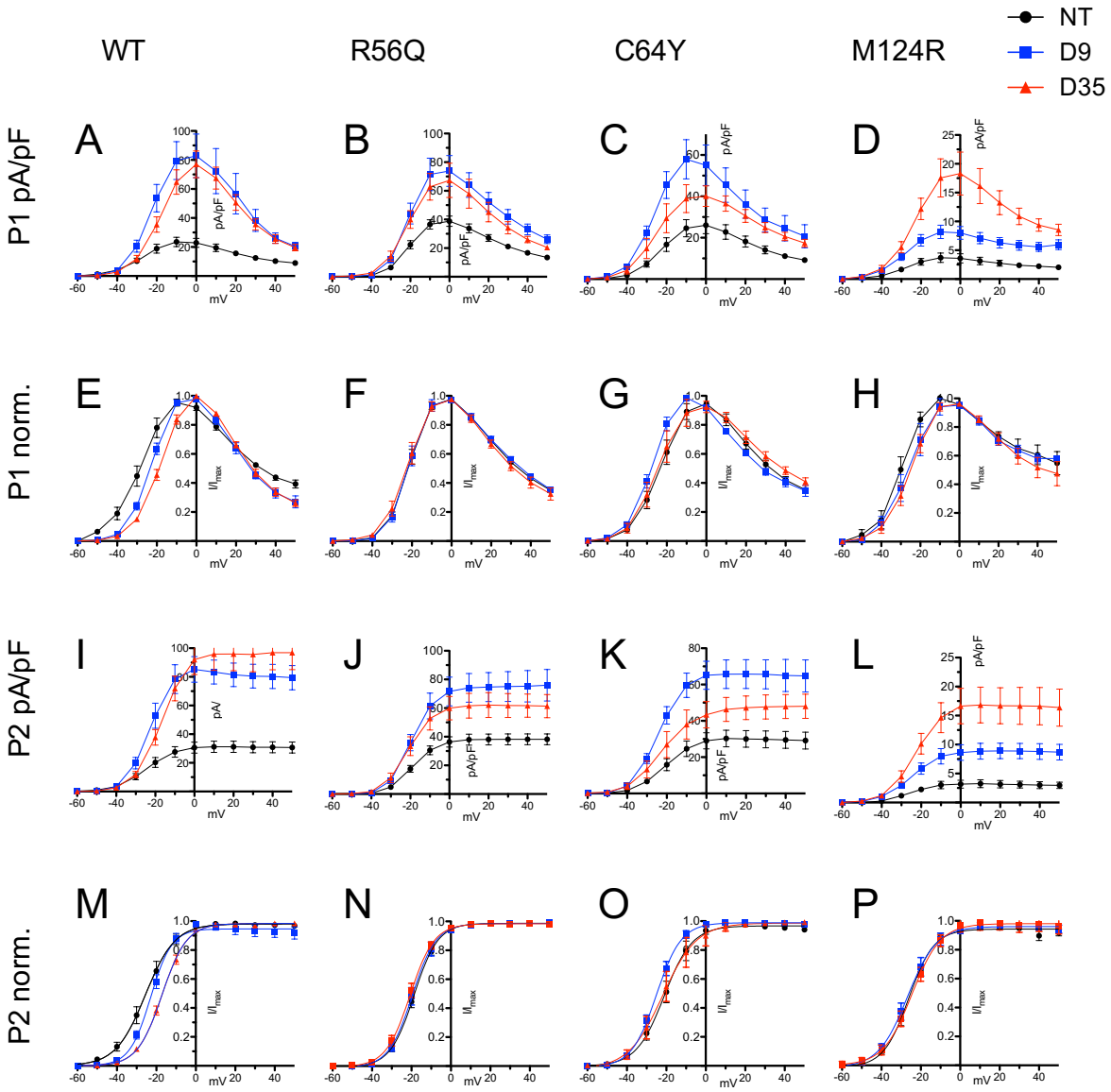

Figure 8: Drug-induced changes in steady-state activation & inwardly rectifying I-V relationship. hERG expressing cells (WT, R56Q, C64Y, M124R) were treated overnight either DCEBIO (D9) or anagrelide (D35). Sample traces and voltage protocol are outlined in Figure 7. Bell shaped I-V curve showing inward rectification was generated from extracting peak current at the end of the P1 pulse from every sweep, and plotted as current density (A-D) and normalized current (E-H). Steady-state activation I-V was generated from peak tail currents observed at the P2 pulse, plotted against previous P1 voltage, for both current density (I-L) and normalized current (M-P). NT represents no treatment. Points represent mean ± S.E.M (*n*=7-15).

Effect of drugs on rates of deactivation

To determine how DCEBIO (9) and anagrelide (35) affect the rate of $K_v11.1$ deactivation, WT and PAS domain mutants (R56Q & C64Y) were studied using a two-step voltage protocol (Fig. 9 inset; see *methods*) following overnight treatment with each drug at 2 μM. Decay of peak tail current at hyperpolarizing P2 pulse was fit with a bi-exponential function (Eq. 5, n=2). Duration of P2 pulse was measured to be three times the slowest time constant, to ensure complete encapsulation of bi-exponential decay. Both slow and fast time constants were extracted as a measure of slow and fast $K_v11.1$ deactivation (Ng *et al*. 2011) as $K_v11.1$ transitions from the open (peak of tail current) to the closed (end of P2 pulse) gating state. Fast and slow time constants were then plotted against P2 test potential (Fig. 10 A-C). hERG slow deactivation has been previously characterized to be prominent at more depolarizing potentials, while channel fast deactivation shows dominance at more hyperpolarizing potentials (Ng *et al*. 2011; Vandenberg *et al*. 2012). For each $K_v11.1$ population, fast channel deactivation was measured at -110 mV (Fig. 10 G-H), and slow channel deactivation was measured at -60 mV (Fig. D-F); where each transition rate has been observed to be most dominant (Vandenberg *et al.* 2012). No statistical difference (ANOVA, $p>0.05$) for mean fast and slow time constants were observed between DCEBIO, anagrelide, and no treatment control for WT (Fig 10 D&G) and C64Y (Fig. F&I). A one-way ANOVA measured between DCEBIO (357.58 ± 18.39; *n*=6), anagrelide (440.54 ± 49.91 ms; *n* =5), and no treatment control (320.00 ± 20.94 ms; *n*=13) for PAS domain mutant R56Q (Fig. 10E) revealed a significance amongst mean slow time constants between experimental conditions ($F(3)=4.297$, $p=0.0273$). A Dunnett's multiple comparison test, performed post-hoc, revealed that differences observed between mean slow time constants in

ANOVA when comparing anagrelide-treated cells and no treatment control (*). Dunnett's multiple comparison test revealed no significant difference between mean slow time constant of DCEBIO-treated cells (n=6) and no treatment (n=13) for R56Q post-hoc. As shown for WT and C64Y, there is no significant difference between mean fast time constants between groups DCEBIO (94.46 ± 14.00 ms; n=6), anagrelide (104.68 ± 27.91 ms; n=5), and no treatment (79.46 ± 18.33 ms; n=13) in R56Q (Fig. 10H; ANOVA, $p>0.05$).

Together, this suggests that DCEBIO and anagrelide do not significantly affect hERG deactivation kinetics (fast and slow) in WT and moderate gating PAS domain mutant C64Y. However, anagrelide does cause a minor, but significant, increase in slow gating kinetics in severe kinetic PAS domain mutant R56Q, without affecting fast channel deactivation. Recorded currents from severe trafficking mutant M124R were small, and the signal to noise ratio was too high to accurately fit currents with a bi-exponential function. Thus, it is inconclusive whether DCEBIO or anagrelide affect rates of deactivation for M124R.

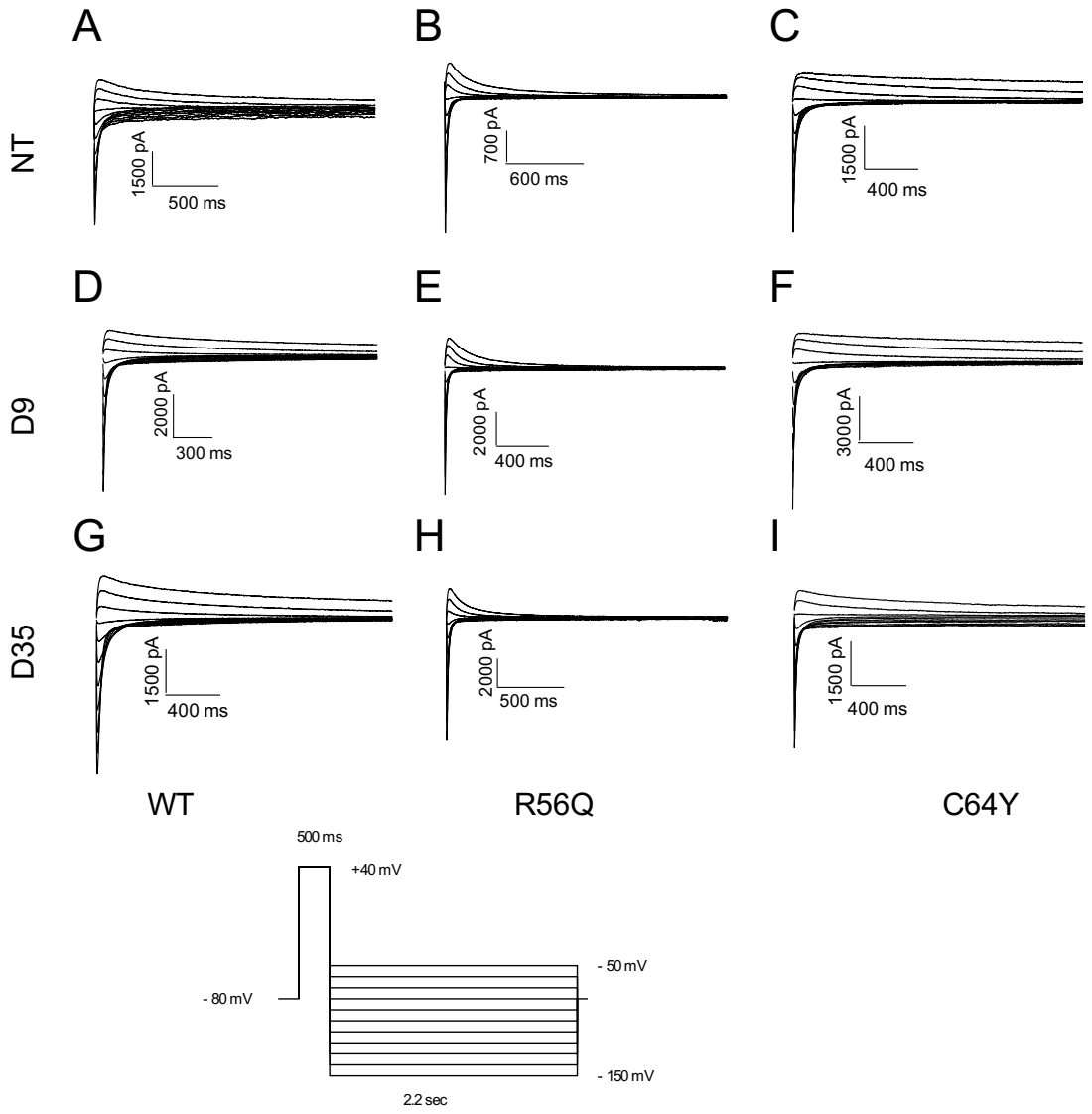

Figure 9: Drug-induced sample traces of rates of deactivation of WT and mutant $K_v11.1$. Sample traces of $K_v11.1$ currents recorded from a two-step voltage protocol (inset). Cells stably expressing WT (column 1), R56Q (column 2), or C64Y (column 3), were stimulated with a two-step voltage protocol. From a baseline of -80 mV, cells were depolarized to +40 mV for 500 ms (P1 pulse), and then hyperpolarized in incremental -10 mV pulses, ranging from -50 to -150 mV for 2.2 seconds (P2 pulse). Cells were studied following overnight treatment of DCEBIO (D9; D-F), anagrelide (D35; G-I) or no treatment (NT; control; A-C). Data are reduced 50-fold.

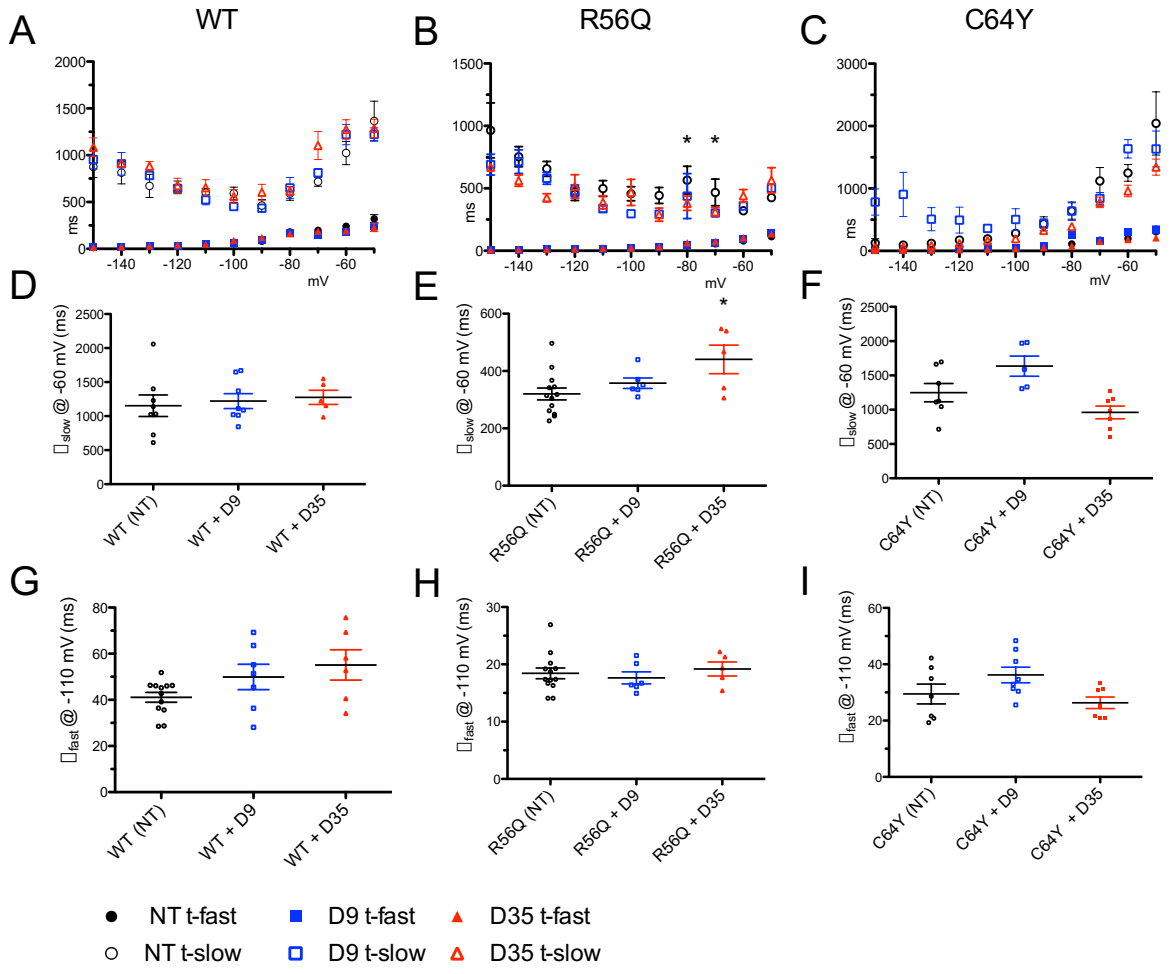

Figure 10: Effect of drugs on fast and slow rates of $K_v11.1$ deactivation.
Summary of rates of deactivation gating for WT (A), R56Q (B), and C64Y (C) after overnight treatment with either DCEBIO (D9) or anagrelide (D35). Voltage protocol is outlined in Figure 9, and summarized in *methods*. Slow time constants measured at -60 mV for each population and condition is summarized (D-F). Fast time constants measured at -110 mV for each population and condition is summarized (G-H). Each datum point represents a unique cell with horizontal bars representing mean ± S.E.M (*n*= 5-13). Statistical significance measured post-hoc are indicated by *.

Effect of drugs on rates of inactivation

To measure any changes in the rapid rate of inactivation of K_v11.1 due to treatment with DCEBIO (9) or anagrelide (35), cells stably expressing either hERG or PAS domain mutant (R56Q or C64Y) were treated overnight with the drug of interest at 2 μM. Using the patch clamp technique, rates of inactivation were then characterized by measuring decay of K_v11.1 current from cells exposed to a three-step voltage protocol (Smith *et al*. 1996). Since the rapid inactivation of K_v11.1 supersedes channel opening (Kiehn *et al*. 1999), it is crucial to use a more complex voltage protocol (three steps) to electrically manipulate K_v11.1 gating states, and time of kinetic measurement, to ensure proper measurement of channel inactivation. From a baseline of -90 mV, cells were forced to transition from the closed, to the open, and then the inactivated state. First cells were depolarized to +40 mV (P1) for 500 ms and then hyperpolarized to -90 mV for 30 ms (P2), where channels quickly transition from the inactivated to the open state (Kiehn *et al*. 1999). The duration of this hyperpolarizing step is sufficiently short to permit channel rapid recovery from inactivation, but too short for slow channel deactivation to occur (Smith *et al.* 1996; Vandenberg *et al.* 2012). Consequently, at the end of the P2 step, channels are in the open state. Cells then experienced a series of +10 mV incremental depolarizing steps, from -60 mV to +80 mV, for 250 ms (P3) where channels transition from the open to the inactivated gating state (Fig. 11 inset). Rates of inactivation were measured by fitting the decay of current during the P3 step, as channels transition from the open (consequence of preceding short P2 pulse) to the inactivated state, with a single exponential (Eq. 5, n=1; Fig. 11). Time constants measured during P3 steps, ranging from -10 to +80 mV, were plotted against their respective depolarizing voltage (Fig. 13 A-C, filled symbols). Rates of inactivation are plotted with rates of recovery from

inactivation (see *methods*), since it has been previously shown the observed rate constants for inactivation and recovery from inactivation are in fact the sum of the unidirectional rate constants at a given voltage (Wang *et al.* 2011; Vandenberg *et al.* 2012). The "observed" rate constant, however, is increasingly dominated by rates of inactivation at more depolarizing voltages (≥ -10 mV), while at increasingly hyperpolarizing voltages (≤ -10 mV), rates of recovery from inactivation dominate channel gating. Plotted together, this gives rise to a distinguishable bell-shaped curved (Wang *et al*. 2011).

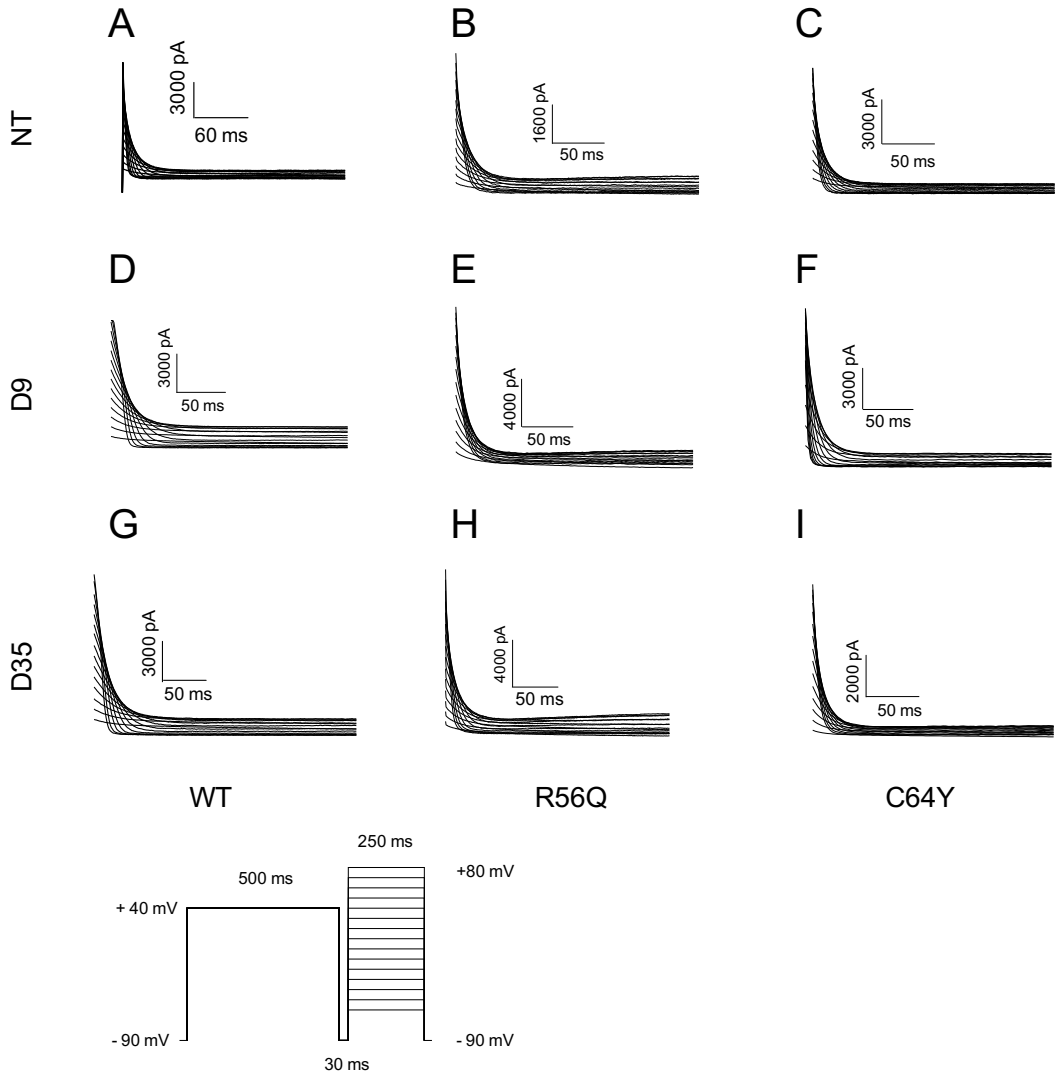

Figure 11: Drug-induced sample traces of the rates of inactivation of $K_v11.1$.
Sample traces of $K_v11.1$ currents recorded from a three-step voltage protocol (inset). Cells stably expressing WT (column 1), R56Q (column 2), or C64Y (column 3) were depolarized from a baseline of -90 mV to +40 mV for 500 ms (P1 pulse), then hyperpolarized to -90 mV for 30 ms (P2 pulse), and then depolarized in incremental +10 mV steps, ranging from -60 to +80 mV for 250 ms. Cells were studied following overnight treatment of DCEBIO (D9; D-F), anagrelide (D35; G-I) or no treatment (NT; control; A-C). Data are reduced 25-fold.

Rate constants measured from P3 pulses ranging from -10 to +80 mV with WT (Fig. 13A; *n*=4-11) and PAS domain mutants R56Q (Fig. 12B; *n*=5-15) and C64Y (Fig. 13C; *n*=7-10) did not statistically differ from no treatment control (*n*=9-15; within each channel population) when treated overnight with either DCEBIO (*n*=4-9) or anagrelide (*n*=6-10; ANOVA, $p>0.05$). As mentioned, time constants extracted from single exponential fit are in fact the sum of two unidirectional rate constants (rate of inactivation and recovery from inactivation), thus time constants at a more depolarizing (+60 mV) step, where channel inactivation has been shown to be dominant (Wang *et al*. 2011), have been highlighted (Fig. 13 D-F). Even using more resolute analysis at +60 mV did not reveal any statistical difference was measured between drug treatment conditions and control for each of the populations studied (two-way *t*-test, $p>0.05$).

Since neither DCEBIO or anagrelide alter $K_v11.1$ rate constants, particularly those measured at more depolarizing voltages, it can be inferred that overnight treatment of either drug does not modulate $K_v11.1$ channel inactivation in wild type and PAS domain mutants.

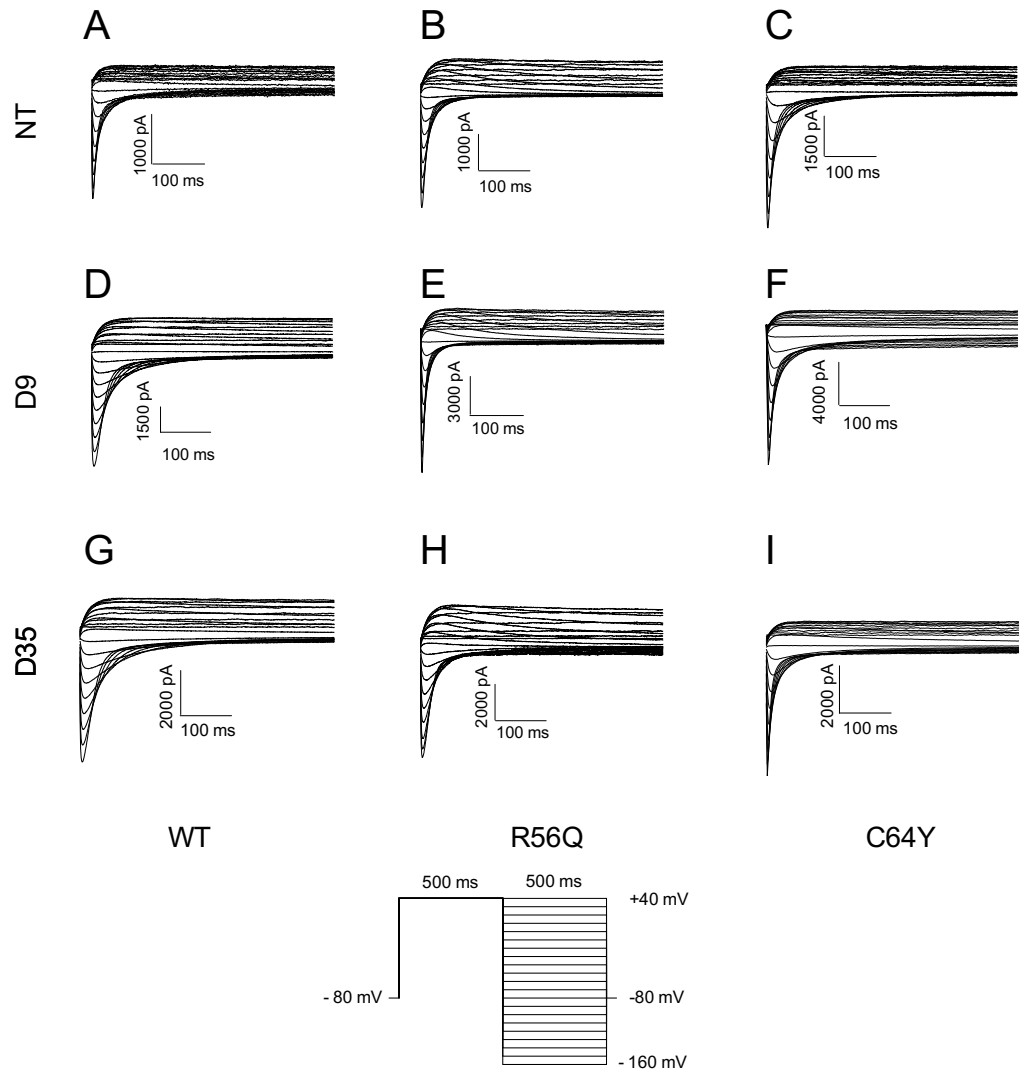

Figure 12: Drug-induced sample traces of $K_v11.1$ recovery from inactivation & steady-state inactivation.

Sample traces of $K_v11.1$ currents recorded from a two-step voltage protocol (inset). Cells stably expressing WT (column 1), R56Q (column 2), or C64Y (column 3) were depolarized from a baseline of -80 mV to +40 mV for 500 ms (P1 pulse), and then hyperpolarized with incremental -10 mV steps, ranging from +40 mV to -160 mV, for 500 ms (P2 pulse). Cells were studied following overnight treatment of DCEBIO (D9; D-F), anagrelide (D35; G-I) or no treatment (NT; control; A-C). Data are reduced 40-fold.

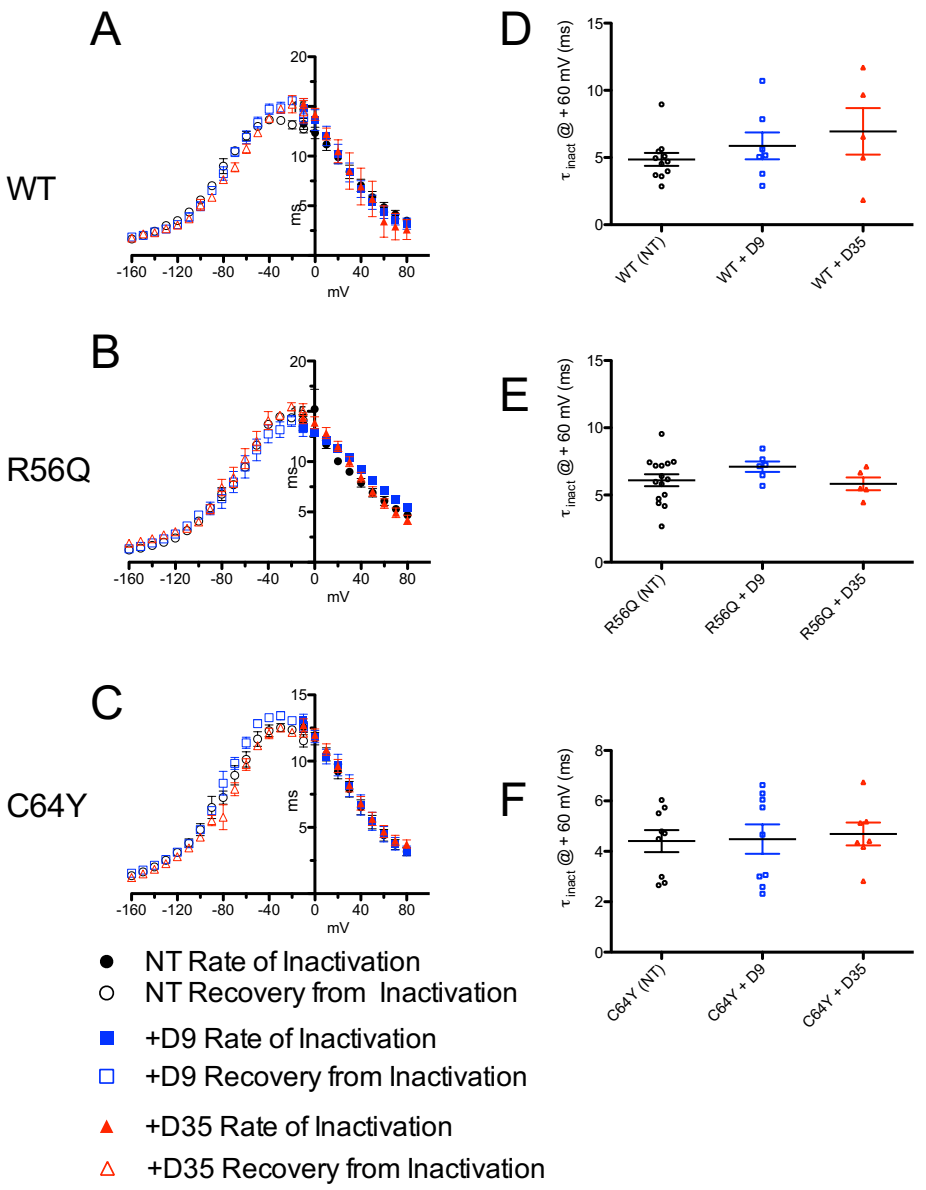

Figure 13: Effect of drugs on rates of inactivation & recovery from inactivation of $K_v11.1$. Summary of rates of inactivation & recovery from inactivation gating for WT (A), R56Q (B), and C64Y (C) after overnight treatment with either DCEBIO (D9) or anagrelide (D35). Voltage protocol measuring time constants of inactivation (filled symbols) is outlined in Figure 10, recovery from inactivation (open symbols) is outlined in Figure 13, and both are summarized in *methods*. Time constant of inactivation measured at +60 mV depolarizing P3 pulse for each population and condition is highlighted (D-F). NT represents no treatment control. Each datum point represents a unique cell with horizontal bars representing mean ± S.E.M (*n*= 4-15 for inactivation; *n*=5-13 for recovery from inactivation).

Effect of drugs on rates of recovery from inactivation

To determine whether drugs DCEBIO (9) or anagrelide (35) had any modulatory effects on the rapid recovery from inactivation of $K_v11.1$, WT and PAS domain mutants (R56Q & C64Y) were treated overnight with either drug, then studied using the patch clamp technique. A two-step voltage protocol was used to characterize channel rates of recovery from inactivation (Wang *et al.* 2010). From a baseline of -80 mV, cells were stepped to +40 mV for 500 ms (P1 pulse). This depolarization induces channels at the cell surface to transition from the closed, to open and then inactivated state (Smith *et al.* 1995). Cells were then hyperpolarized in incremental -10 mV voltage steps, ranging from +40 mV to -160 mV, for 500 ms (P2 pulse; Fig. 12 inset). Recorded tail currents from every P2 step were fit bi-exponentially (Eq. 5, n=2) from the base of the tail current to the onset of plateau of the decaying slope (Fig 13; Vandenberg *et al*. 2012). Since hyperpolarizing P2 steps force channels from the inactivated state (due to P1) to transition to the open, and then closed state, fast time constants of bi-exponential fit measure the fast rates of recovery of channel inactivation (upstroke of tail current (Trudeau *et al*. 1995; Vandenberg *et al*. 2012). Fast time constants from bi-exponential fit of P2-induced tail currents (from -10 to -160 mV) were plotted against their respective voltage to study rates of recovery from inactivation (Fig. 13 A-C, open symbols). As previously mentioned, observed rate constants are the sum of unidirectional rate constants for rates of inactivation and recovery from inactivation (Wang *et al*. 2011), where rates of recovery from inactivation governs observed rate constant at more hyperpolarizing potentials (≤ -10 mV). Consequently, rate constants were only plotted in the range of -160 to -10 mV, where recovery from inactivation significantly influences observed rate constant.

Following overnight treatment, there were no significant differences of fast time constants between DCEBIO-treatment (*n*=5-9), anagrelide-treatment (*n*=6-10) or no treatment control (*n*=9-13) at all measured at the P2 step (ANOVA, p>0.05). These findings are true in cells stably expressing WT (Fig. 12A; *n*=6-13), or PAS domain mutants R56Q (Fig. 13B; *n*=5-13), and C64Y (Fig. 13C; *n*=7-9). Together, this indicates that neither drug affects the rate of recovery from inactivation in WT or PAS domain mutant K_v11.1 channels.

Effect of drugs on steady-state inactivation

To determine if DCEBIO (9) or anagrelide (35) affect K_v11.1 steady-state inactivation, currents recorded from cells expressing WT and PAS domain mutant (R56Q & C64Y) channels following a two-step voltage protocol were studied. Steady-state inactivation is measured using the same voltage protocol used to measure rates of recovery from inactivation (Fig. 12; see *methods*), followed by a different analysis. Steady-state inactivation is analyzed as channels transition from the inactivated, to open, to closed state during the hyperpolarizing P2 pulse (Sanguinetti *et al*. 1990; Sanguinetti *et al*. 1995). Peak tail currents were plotted against their respective voltage as current density (Fig 14 A-C) and normalized current (Fig. 14 D-F). To better study the kinetics of steady-state inactivation normalized currents were compared at every voltage step to study steady-state inactivation. Normalized tail currents of WT (Fig. 14D; *n*=8-11) and PAS domain mutants R56Q (Fig. 14E; *n*=5-15) and C64Y (Fig. 14 F; *n*=7-9) did not significantly differ from +40 to -160 mV, between overnight treatment of DCEBIO (*n*=6-9), anagrelide (*n*=5-7), and no treatment control (*n*=9-15). DCEBIO and anagrelide do not alter steady-state inactivation kinetics in WT and PAS domain mutants.

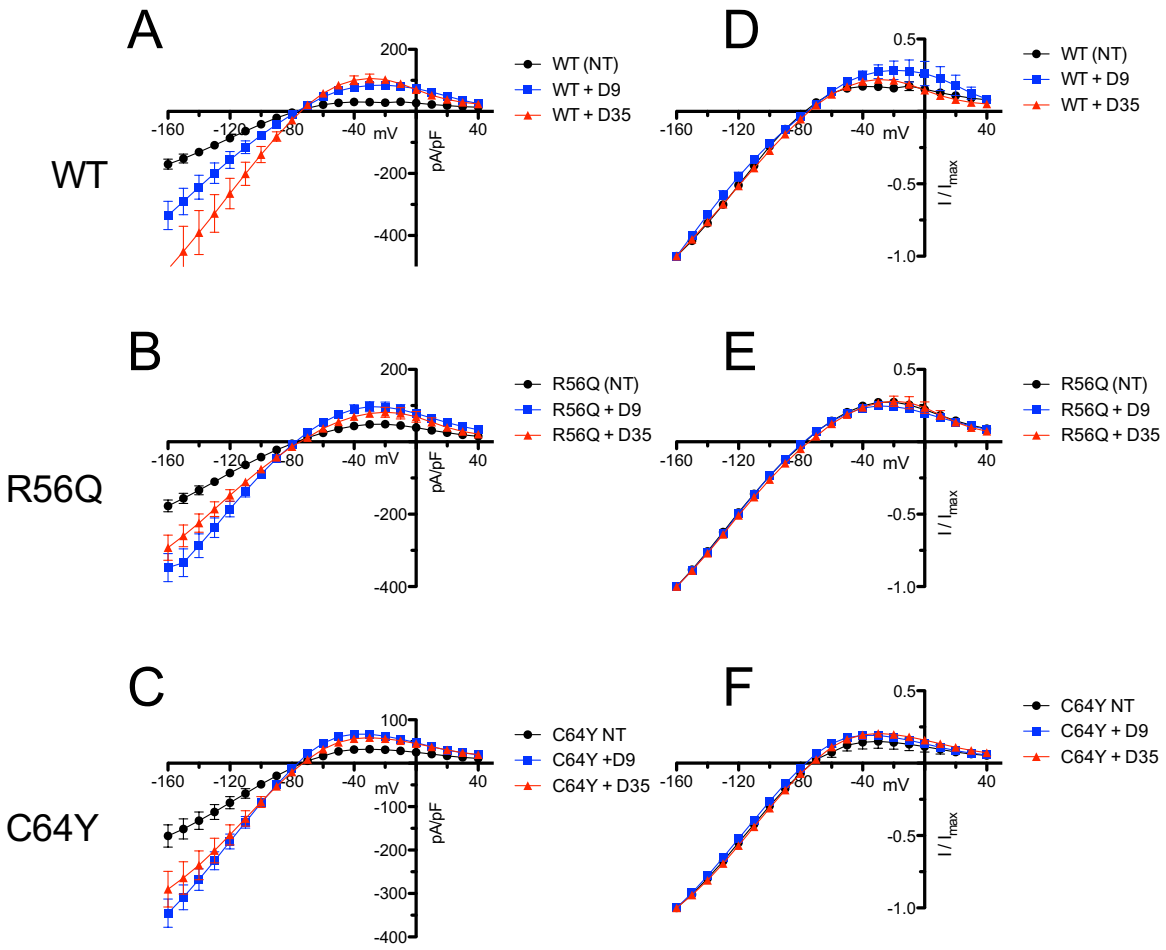

Figure 14: Effect of drugs on steady-state inactivation of $K_v11.1$.
Summary of rates of inactivation & recovery from inactivation gating for WT (row 1), R56Q (row 2), and C64Y (row 3) after overnight treatment with either DCEBIO (D9) or anagrelide (D35). Voltage protocol measuring peak tail currents is outlined in Figure 13, and is summarized in *methods*. Peak tail current measured during P2 pulse is plotted against voltage step as current density (A-C) and normalized current (D-F). NT represents no treatment control. Each datum point represents a unique cell with horizontal bars representing mean ± S.E.M (*n*= 5-15).

Effect of drugs on functional cell-surface expression

To measure if overnight treatment of DCEBIO (9) or anagrelide (35) caused any changes in cell surface expression of K_v11.1, WT and PAS domain mutants (R56Q, M124R, & C64Y) were treated overnight with both drugs at 2 μM and studied with the patch clamp technique. Cells were stimulated using the same two-step voltage protocol invoked to study rates of recovery from inactivation and steady-state inactivation (Fig. 12), however, only data recorded from the -120 mV P2 voltage step was used to measure changes in functional expression of K_v11.1 at the cell surface. It has previously been shown that analysis of K_v11.1 at the cell surface is best studied using peak tail current analysis. (Trudeau *et al.* 1995; Smith *et al.* 1996). Due to the voltage dependence of K_v11.1, a large depolarizing P1 pulse (+40 mV) held for a sufficiently long duration, ensures that all the channels at the cell surface transition from the closed state to the activated, and end the P1 pulse in the inactivated state. The subsequent hyperpolarizing P2 pulse will stimulate channels to rapidly recover from inactivation (inactivated to open state) and then deactivate (open to closed state) shown electrophysiologically as a tail current (Fig. 13). Thus, the number of channels that are available to recover from inactivation, and conduct current, are those in the inactivate state due to the previous P1 pulse; and at P1 of +40 mV, all channels are assumed to be in the inactivated state. Again, due to the voltage dependence of K_v11.1, a sufficiently hyperpolarizing pulse is required to ensure all channels are induced to recover from inactivation (Smith *et al.* 1996). Dr. Jamie Vandenberg, and colleagues, have shown that a P2 voltage step of -120 mV is sufficiently large to warrant recovery from inactivation from all functional channels, and consequently, allow for accurate quantification of functional K_v11.1 channels at the cell surface (Vandenberg *et al.* 2012). However, slow channel

deactivation occurs during channel recovery from inactivation (upstroke of tail current). Thus, to ensure an accurate quantification of hERG at the cell surface, channel deactivation must be corrected (Fig. 15). Using the extrapolation method, decay of the peak tail current is fit with a single exponential function (Eq. 5, n=1; fitting fast channel deactivation) and extrapolated back to the onset of the P2 pulse (Fig. 15C; Vandenberg *et al*. 2012). The current measured at the intersection of the fit and the start of the P2 step is the theoretical value of current magnitude if not deactivation did not occur during recovery from inactivation.

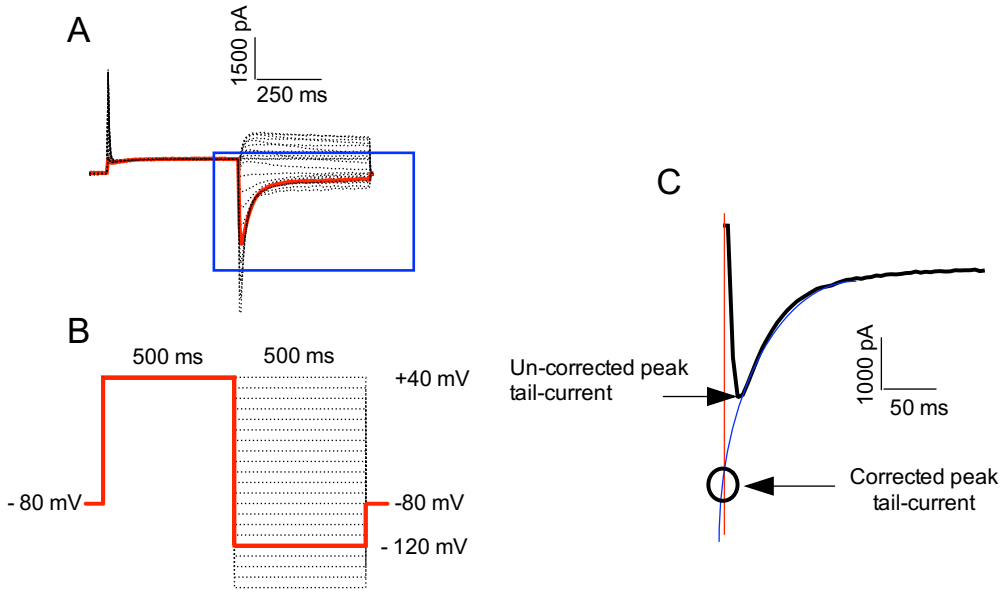

Figure 15: Extrapolation method for correction of deactivation in peak tail current analysis. Graphic outline of $K_v11.1$ peak tail current measurement before and after correction for channel deactivation. Full sample trace of WT $K_v11.1$ (A) from two-step voltage protocol (B; see *methods*). Red line in panels A & B highlight trace from -120 mV P2 pulse. Inset of peak tail current at -120 mV from A is highlighted (C). Single exponential fit of current decay (blue line) is extrapolated back to onset of P2 pulse (vertical red line). Current at intersection of onset and single exponential fit is peak tail current magnitude corrected for deactivation. Data are reduced 100-fold.

Following proper correction for channel deactivation, $K_v11.1$ current density measured at -120 mV was plotted for WT, R56Q, M124R, and C64Y after either DCEBIO, anagrelide, or no treatment (control). In WT (Fig. 16A), DCEBIO and anagrelide both significantly increased mean corrected peak tail current density at -120 mV to 248.1 ± 3.12% and 249.9 ± 3.77% (respectively) of no treatment control. In R56Q (Fig. 16b), DCEBIO and anagrelide both significantly increased mean corrected peak tail current density at -120 mV to 213.9 ± 3.11% and 143.5 ± 1.31% (respectively) of no treatment control. In M124R (Fig. 16C), DCEBIO and anagrelide both significantly increased mean corrected peak tail current density at -120 mV to 349.29 ± 3.50% and 692.4 ± 7.80% of no treatment control. In C64Y (Fig. 16D), DCEBIO and anagrelide both significantly increased mean corrected peak tail current density at -120 mV to 225.82 ± 2.01% and 236.54 ± 2.94% (respectively) of no treatment control.

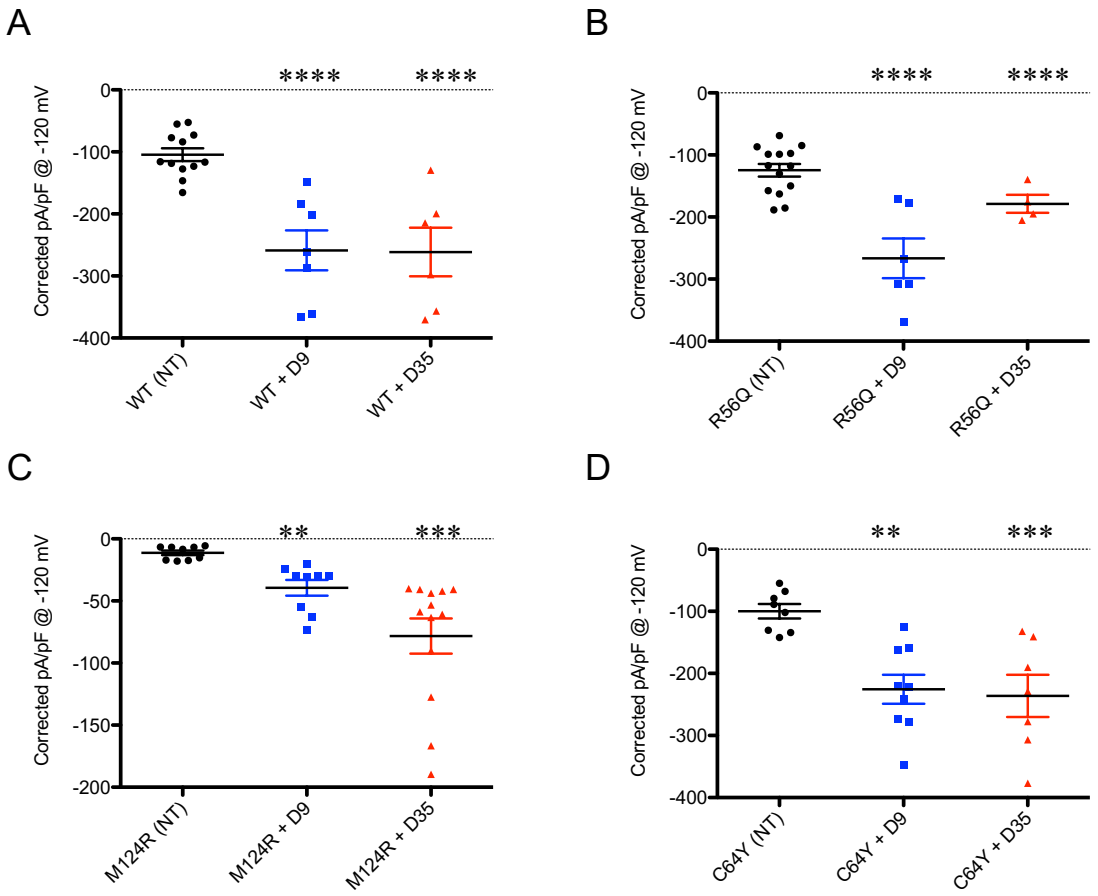

Figure 16: Effect of drugs on $K_v11.1$ cell-surface expression
Peak tail currents measured at a -120 mV hyperpolarizing voltage step (Fig. 13 & 15; see *methods*) in WT (A), R56Q (B), M124R (C), and C64Y (D) after overnight treatment of either DCEBIO (D9) or anagrelide (D35). Plotted is peak tail current density after correction for channel deactivation using the extrapolation method (Fig. 15; see *methods*). NT represents no treatment control. Each datum point represents a unique cell with horizontal bars representing mean ± S.E.M (*n*= 4-14).

In summary, data indicate that both DCEBIO and anagrelide significantly increase mean corrected peak tail current of $K_v11.1$ in WT, R56Q, M124R, and C64Y. This suggests that both drugs upregulate functional channels at the cell surface in WT and PAS domain mutant expressing cells. Further, when corrected peak tail current treated by DCEBIO is plotted against control and forced through the origin, the data followed a linear trend (Fig. 17A; slope = 2.276 ± 0.09106, T(3)= 25.00, p =0.0001). When fit for linear regression, and not fit through the origin, 98% of the variability in upregulated peak tail current induced by DCEBIO is attributed the non-treated tail currents found in no treatment control (R^2=0.9818). Successful fit of peak tail current before vs. after overnight treatment of DCEBIO on various expression forms of $K_v11.1$ (WT & mutants) indicates a potential model for how this compound acts. This suggests that DCEBIO upregulates functional PM expression of $K_v11.1$ depending on the initial, untreated quantity of $K_v11.1$ expressed at the cell surface. Further, this model could be applied to predict the effects DCEBIO would have on untested $K_v11.1$ mutants. Although this linear trend is not observed for anagrelide (data not shown), anagrelide's upregulation in severe trafficking mutant M124R was sufficiently high to rescue WT phenotype (two tailed T(23)=1.484, p=0.1513 > 0.05). Summaries of quantification, both absolute and relative, are outlined in Table 3.

hERG Channel	Mean peak tail-current @ -120 mV ± SEM (pA/pF)	Peak tail-current vs. control NT (%)	Peak tail-current vs WT NT (%)	Sample size
WT (NT)	-104.6 ± 10.35	100	100	12
WT + D9	-258.7 ± 32.28 ****	248.1	248.1	7
WT + D35	-261.4 ± 39.06 ****	249.9	249.9	6
R56Q (NT)	-124.6 ± 10.30	100	119.1	14
R56Q + D9	-266.5 ± 32.03 ****	213.9	254.8	6
R56Q + D35	-178.8 ± 14.50 ****	143.5	170.9	4
C64Y (NT)	-99.90 ± 11.57	100	95.51	8
C64Y + D9	-225.6 ± 23.27 **	225.82	215.7	9
C64Y + D35	-236.34.00 ***	236.54	225.6	7
M124R (NT)	-11.30 ± 1.81	100	10.80	9
M124R + D9	-39.47 ± 6.349 **	349.29	37.73	9
M124R + D35	-78.24 ± 14.12 ***	692.4	74.8	13

Table 3: Summary of mean peak K_v11.1 tail-current measured at -120 mV corrected for deactivation.

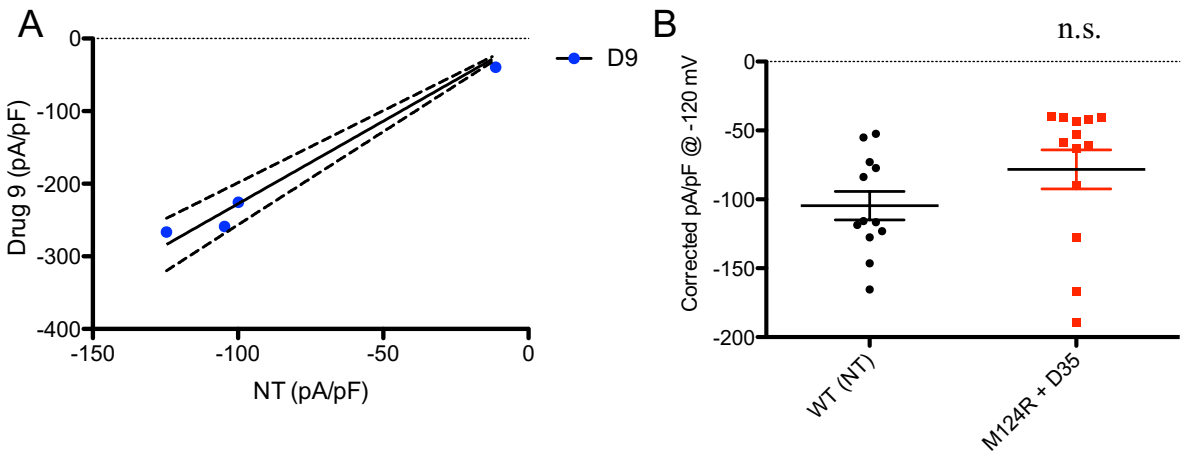

Figure 17: Unique and unexpected effects from drugs on $K_v11.1$ expression.
Corrected peak tail current after overnight treatment of DCEBIO (D9) was plotted against corrected peak tail current of no treatment control (NT) for WT, R56Q, M124R & C64Y (A). Linear regression, forced through the origin, is plotted (solid black line) with 95% confidence intervals for slope (dashed black line). Scatter plot of corrected peak tail current after overnight treatment of anagrelide (D35) in M124R and WT no treatment control (NT). Each datum point represents a unique cell with horizontal bars representing mean ± S.E.M (*n*= 12-13; B).

Discussion

There are currently no known drugs that can upregulate cell-surface expression of functional hERG without blocking the channel pore. It has previously been hypothesized that mechanistically, upregulation of rapidly activating, delayed rectifier K^+ channel (I_{Kr}) may be sufficient for anti-arrhythmic therapy, particularly LQT2 (Chianvimonvat *et al.* 2017). Preliminary data provided by Brian Foo (and colleagues) using a high throughput cell surface ELISA screen identified 153 compounds that can upregulate hERG cell surface expression (Fig. 1). Through development of appropriate criteria, drugs were narrowed down to a smaller pool of 57 potential rescuing compounds (Fig. 3). Analysis of currents conducted by WT hERG expressing cells acutely treated with artesunate (D1), one of the 57 compounds, was performed using electrophysiological techniques and showed that artesunate does not the block channel pore (Fig. 4A & 5A). Data also revealed that artesunate does not significantly modulate $K_v11.1$ current magnitude acutely (15-minute time scale; Fig. 4A). Patch clamp experiments showed that overnight treatment of artesunate demonstrated approximately a 2.7-fold increase in current density in WT hERG (Fig. 6F), without any significant changes in activation gating or pore charge (Fig. 6G). Preliminary cell surface ELISA experiments (Brian Foo) indicated an upregulation of hERG of 1.20-fold relative to control. This demonstrates that artesunate does in fact upregulate functional WT $K_v11.1$ at the cell surface, without affecting activation gating. Previous studies have shown that when ingested in humans, artesunate is rapidly hydrolyzed to dyhydroartemisinin, its active metabolite. Although the pharmacokinetics of metabolism of artesunate are variable amongst humans (particularly in healthy vs. unhealthy patients), overall drug metabolism occurs on a scale of hours (1-2 hours; HSDB artesunic acid). Since the earliest

this study identifies $K_v11.1$ upregulation is overnight, artesunate cannot qualify as a potential therapy for LQT2, since its fast metabolism renders it in a modified form (dihydroartemesinin). Future experiments should consider identified the minimum time for effective upregulation of artesunate and/or repetition of the conducted analyses of its metabolite.

An additional screen for $K_v11.1$ pore block was conducted by Brian Foo. Although a myriad of potential drug candidates were found to upregulate cell surface hERG in both WT and certain mutants (PAS domain and/or G601S; data not shown), it is crucial that any potential therapy for LQT2 by hERG upregulation does not block the channel pore. Any such compound would only exacerbate the action potential in LQT2 patients. This could also induce signs of acquired LQT2 in healthy individuals Ishii and colleagues have previously studied a series of compounds that upregulate hERG assembly, but also bind the channel pore (Ishii *et al*. 2003; Chadwick *et al.* 2005). This study identified that compound E4031 upregulates WT hERG production but binds the channel at residue 656 (phenylalanine). This study also revealed that point mutations at F656 prevents E4031 binding, and thus prevents channel upregulation. Cell surface ELISA experiments revealed that five compounds (droperidol, DCEBIO, danazol, AC-93253 iodide, zardaverine, and anagrelide) equally upregulate cell surface expression of both WT (NT) and WT-F656A point mutated hERG (Fig. 2). This suggests that all five compounds can increase expression of $K_v11.1$ at the cell surface and do not block the channel pore in the commonly exhibited E4031-fashion (Ishii *et al*. 2003) and thus highlights the potential of these drugs as therapeutic candidates.

To further investigate, electrophysiological studies were executed to determine if acute treatment of these drugs (15 minutes) would 1) restrict ion conductance through the channel, and

2) alter channel functionality (current magnitude). From this, DCEBIO, danazol, and anagrelide were found to not block the K_v11.1 channel pore in WT cells, compared to no treatment, positive control. In contrast, droperidol and AC-93253 iodide block WT channel conductance, showing no statistical difference from E4031 treatment (negative control; Ishii *et al*. 2003; Fig. 5). Compounds which upregulate but block K_v11.1 conductance represent an underlying cause for acquired LQT2 (Robertson *et al.* 2006). Thus, although droperidol and AC-93253 may upregulate K_v11.1 trafficking to the cell membrane, studies involving these two compounds were terminated. Further, of the compounds that did not block channel conductance, none acutely (≤15 minutes) upregulate WT K_v11.1 current density, and thus cell surface expression and functionality (Fig. 4). In fact, all four "non-blockers" appear to cause a minor reduction in current density. This becomes obvious when treated currents are normalized to paired, un-treated control current densities (Fig. 5). The observed reduction in current density is assumed to be a consequence of holding whole-cell voltage clamp configuration for more than 15 minutes. Although offline leak subtraction was performed, holding whole-cell for such a long duration negates the assumptions made: that leak is constant throughout all recordings, and consequently, a reduction in current density following long patch durations was expected due to compromise of the integrity of the patch seal. Acutely treating WT K_v11.1 with each drug revealed that artesunate, DCEBIO, danazol and anagrelide do not block the channel pore of K_v11.1, do not hinder channel conductance, and do not acutely modulate channel trafficking to the cell surface. Upon further analysis of these compounds, their "non-blocking" characterization makes them excellent candidates for treatment of LQT2, potentially via hERG upregulation. Moreover, acute electrophysiological analysis of WT K_v11.1 also revealed that exclusive use of cell surface

ELISA of F656A point mutated hERG is insufficient to predict channel block. This is inferred by the false-negative result of artesunate, and the false-positive characterization of droperidol and AC-93253 iodide from cell surface ELISA (Fig. 2). It is suggested that future use of this technique for determining channel block be used in tandem with electrophysiological/functional analysis.

To characterize the four remaining drug candidates, electrophysiological analysis of various hERG expressing cells were studied. WT hERG expressing cells were first studied to determine if preliminary cell surface ELISA findings (Fig. 3) could be replicated and substantiated in upregulation of current density from patch clamp experiments. Peak tail current analysis revealed a greater increase in WT $K_v11.1$ at the cell surface when treated with either DCEBIO or anagrelide than the observations made with cell surface ELISA. In fact, this was true for PAS domain mutants C64Y and M124R (Table 3). No cell surface ELISA was conducted on R56Q, and thus the data could not be compared, however overnight treatment of both anagrelide and DCEBIO also revealed significant functional cell surface increase, relative to control, in PAS domain mutant R56Q. High throughput patch clamp experiments (data not shown; conducted by Dr. Corey Valinsky) revealed that danazol did not significantly increase $K_v11.1$ current; and thus danazol was omitted in subsequent experiments.

Previous studies show evidence that the major cause of LQT2 is deficient $K_v11.1$ trafficking from the endoplasmic reticulum, causing a reduction in the number of functional channels at the cellular membrane (Anderson *et al.* 2006; Robertson *et al*. 2006). Rescue of protein trafficking to the cell surface has been hypothesized to correct $K_v11.1$ current density, restoring healthy cellular function in patients suffering from trafficking-deficient caused LQT2.

The ability for DCEBIO and anagrelide to upregulate $K_v11.1$ current density in all studied hERG expression systems, both WT and PAS domain mutants (Fig. 16; Table 3), demonstrates the potential for both drugs to rescue WT phenotype in patients suffering from either acquired or inherited LQT2. Although the effectiveness of these drugs was not studied *in vivo* systems, it is of interest that severe trafficking mutant M124R (Ke *et al*. 2013) was upregulated. M124R has previously been shown to be one of the most severe, low current expressing hERG mutants, with a known prevalence in Jewish populations (Ke *et al.* 2013; Shushi *et al.* 2005). Hence, prior to any experiments, it was thought that any drug that can rescue M124R could also rescue all the less severe PAS domain trafficking mutants. As expected, untreated M124R cells were observed to express diminutive currents, such that kinetic analysis was impossible in these cells (Fig 7D). Treatment with these drugs, however, corrected currents sufficiently to permit a kinetic analysis. In fact, overnight treatment with anagrelide was sufficiently potent so as to rescue WT expression levels of M124R (Fig. 17B). Although DCEBIO did not show such potency, it did increase M124R currents, and dose response cell surface ELISA studies (performed by Brian Foo; data not shown) revealed that the working 2 μM concentration was only halfway up the sigmoidal curve for DCEBIO, where 2 μM for anagrelide was at maximum $K_v11.1$ upregulation in both WT and mutant T65P. This indicated that theoretically an even greater upregulation, at high working concentrations, of DCEBIO is possible. Notably, not using max working concentration could be one explanation for the inverted effect observed between both drugs and M124R (Fig. 8). An alternative hypothesis is that anagrelide may be working in a manner to raise hERG expression to a certain quantitative value, while DCEBIO works as a corrector based on initial PM expression (as explained by linear regression model). By this assumption, DCEBIO

would be less effective on low PM expressing mutants, such as M124R, than anagrelide, but more effective on milder expression mutants (C64Y, R56Q). In summary, *in vitro* patch clamp studies show that drug-induced cell surface upregulation of functional K_v11.1 channels, no matter the severity of trafficking/expression (whether WT or PAS domain mutants) as a mechanism for therapeutic treatment of LQT2.

The unique gating kinetics of K_v11.1 are essential for proper channel function. Alterations in channel gating have been previously shown to be a major cause for LQT2, and are a staple of mutations in the PAS domain (Chen *et al.* 1999; Gianulis *et al*. 2011; Ke *et al*. 2013; Ke *et al*. 2014). Therefore, it is essential that any potential therapy for LQT2 by functional upregulation does not modulate channel gating. To determine whether DCEBIO or anagrelide affect K_v11.1 kinetics, electrophysiological analysis was used to measure K_v11.1 steady-state activation, activation gating charge, rates of deactivation, rates of inactivation, rates of recovery from inactivation, and steady-state inactivation. The PAS domain has previously been shown to be crucial in channel deactivation kinetics, and therefore in addition to defects in channel trafficking PAS domain mutants commonly exhibit accelerated deactivation kinetics (Schonherr *et al.* 1996; Spector *et* al. 1996; Chen *et al*. 1999; Harley *et al.* 2012). Although altered gating, particularly deactivation, could not be rescued to WT phenotype following treatment of either drug, neither drug further worsened PAS domain mutant gating. This was true in all studied populations including WT and severe gating mutant R56Q (Ke *et al*. 2013). Exceptions to the unaltered gating are two measurements of slow deactivation in R56Q (Fig. 7D). The deactivation kinetics of K_v11.1 are often studied using a single exponential fit (Ke *et al.* 2013; Vandenberg *et al.* 2012). This method of kinetic analysis is often observed when either slow or fast deactivation

is dominant (very hyperpolarized, or very depolarized potentials). This study analyzed both slow and fast gating kinetics to determine whether there were any drug-induced modifications to either gating state (see *methods*), however, it can be justified that differences in slow gating kinetics in R56Q are not drug-related, but in fact caused by poor measurements of the slow component. This is justified since PAS domain mutants have fast gating kinetics (Schonherr *et al*. 1996; Spector *et al*. 1996), of which R56Q presents one of the most severe phenotypes (Ke *et al*. 2013; see *PAS domain*), and thus rapid deactivation is dominant at all voltage steps. In fact, it is not uncommon for deactivation to be measured as done in this study (bi-exponential fit; see *methods*) but to exclusively analyze fast gating (Ke *et al*. 2013), since often slow deactivation time constants lead to inaccurate measurements, particularly when studying PAS domain mutants.

Studies show that optimal rescue of WT phenotype in inherited LQT2 are accomplished by pharmacological agents which can restore both trafficking and gating defects caused by mutations in $K_v11.1$. However, compounds which can rescue channel trafficking, and thus current density without aggravating the gating of $K_v11.1$ have been suggested to be potentially useful in treating less severe gating mutations (Robertson *et al.* 2006; Perry *et al.* 2016). If compounds which strictly rescue $K_v11.1$ trafficking do not alter (nor restore) channel gating, then these drugs could potentially rescue over half the PAS domain mutations, as well as serve as a treatment for patients suffering from acquired LQT2, since the underlying cause for this this disease is reduction in $K_v11.1$ current (Anderson *et al.* 2006; Robertson *et al.* 2006). Hence, in summary the data presented in this study shows that although DCEBIO and anagrelide could not rescue aberrant gating of severe deactivation mutant R56Q, both drugs did not alter hERG

K_v11.1 kinetics, namely deactivation, inactivation and recovery from inactivation in WT and various PAS domain mutants studied in a cellular model system. Together, this indicated that these compounds still possess significant therapeutic potential. To better test the effectiveness of both compounds, it is suggested that AP studies are performed on cells endogenously expressing hERG, such as cardiacmyocytes. Using techniques such as CRIPR would conclude whether DCEBIO or anagrelide can rescue WT AP phenotype in the various PAS domain mutants.

Finally, in addition to functional cell surface upregulation and absence of kinetic modification, this study revealed a final, unpredicted, phenomena for the interaction of DCEBIO and hERG. Peak tail current analysis of DCEBIO-treated K_v11.1 expressing cells (WT, R56Q, C64Y, & M124R) plotted against their respective untreated controls accurately fit a model of linear of regression. This suggests that DCEBIO's upregulatory effect on other PAS domain mutants can be predicted by a linear model. Depending on the quantity of a given hERG mutant at the PM, this linear model provides sufficient evidence for a preliminary quantitative measure of the functional expression of K_v11.1 at cell surface following overnight treatment of DCEBIO. Since it has previously been shown that heterozygote channels with only one WT hERG allele maintain regular channel properties and functionality (Piippo *et al.* 2000), it can be assumed that 50% cell surface expression, or rather current density, is sufficient for channel rescue. With this model, it is theoretically possible to determine in which PAS domain mutants WT expression levels can be rescued by DCEBIO. If these findings could be substantiated in a *in vivo* model, this would be critical in accelerating treatment of inherited LQT2.

Conclusion & Summary

In summary, preliminary analysis using various variations of cell surface ELISA identified a population of compounds from a 5000 drug library that could upregulate cell surface expression of WT and hERG mutants, namely those with point mutations in the PAS domain. In further characterizing some of highlighted compounds, electrophysiological studies showed that treatment of WT $K_v11.1$ channels with artesunate, danazol, DCEBIO and anagrelide does not hinder channel function, and thus does not block the channel pore. Alternatively, droperidol and AC-93253 iodide did block the channel pore and inhibit channel function. Using the whole cell voltage clamp technique, it was possible to study the functional properties of all channels existing at the cellular membrane in cells expressing either WT and PAS domain mutant hERG. Although it was shown that artesunate could upregulate WT $K_v11.1$ current density, it was later uncovered that the drugs therapeutic potential would need to be substantiated in its metabolized form: dihydroartemisinin. Although it is possible for rapidly metabolized compounds to rectify the transient phenotypes observed in acquired forms of LQT2, this study limits the effect of the drug to overnight (18-24 hours) and the body metabolizes the compound in less than half that time. Follow-up high throughput patch clamp experiments offered no statistical difference in current density, and thus functional channel trafficking in WT $K_v11.1$ treated with danazol. This study revealed that overnight treatment of DCEBIO or anagrelide upregulates functional channel expression at the cell surface without significantly modulating channel gating. Therefore, electrophysiological characterization of DCEBIO and anagrelide suggests *in vivo* studies to further verify both drugs as pharmacological correctors of trafficking-induced acquired and inherited LQT2.

Acknowledgements

Firstly, I would like to thank Dr. Alvin Shrier, McGill University's Faculty of Medicine, and GEPROM for their financial support throughout my degree.

I would like to thanks McGIL HTS facility for assisting in managing the drug library.

I would like to thank Adam Sherman for his design, construction, and technical support in the patch-clamp apparatus used to conduct my experiments.

I would like to thank my thesis committee, composed of Dr. John Hanrahan, Dr. Gergely Lukacs and Dr. Terry Hebert for their guidance and constructive criticism of my research. Additionally, I would like to thank Dr. Ursula Stochaj for sitting as the GSAAC member in my final thesis presentation. Additionally, I would like to thank my thesis reviewer, Dr. Robert Dumaine for his constructive criticism and positive feedback.

I would also like to wish thanks to the Shrier lab for their continued support, advice, reagents, equipment, and help throughout the completion of my degree. I would like to thank Michael Liben and Dr. Camille Barbier for conducting and analyzing preliminary, molecular biology experiments which inspired my project.

I would like to wish a special thanks to Brian Foo for his experiments and analysis; that without, this project would not exist. His patience, guidance and support were greatly appreciated.

I would like to wish a special thanks to Dr. Corey Valinsky for his patience while teaching me the workings of electrophysiology, the appropriate methods of data analysis, as well as for the work he contributed in the completion of this project.

Finally, I would like to wish a final, and special thanks to Dr. Alvin Shrier for his supervision, guidance, technical support, and editorial help in the completion of my thesis and Master's degree.

Preface & Contribution of Authors

Methodology A – This section was written exclusively by Brian Foo. It includes the methodology for the techniques used by Brian Foo.

Molecular Biology – All data collected and analyzed from molecular and cellular biology techniques was performed and/or supervised by Brian Foo. In text contribution are specifically mentioned. This includes high throughput drug screen, F656A study, and cell surface ELISA. Certain cell surface ELISA data were collected by Michael Liben. Dr. Camille Barbier contributed to some collection for F656A study. All experiments conducted by Brian Foo *et al*. have been labelled as "Results – Part A."

Electrophysiology – All patch clamp data for condition C64Y+D35 was collected by Dr. Corey Valinsky. Analysis for this data were conducted by both Dr. Corey Valinsky and Joshua Solomon. Most, but not all, patch clamp data for conditions M124R+D35 and C64Y NT were collected by Dr. Corey Valinsky. The remaining data were collected by Joshua Solomon. Data analysis was conducted by both individuals. Most, but not all, patch clamp data for conditions WT+D35 was collected by Joshua Solomon; the rest by Dr. Corey Valinsky. Data analysis was conducted by both individuals. Patch clamp data for all other conditions, including the artesunate study and acute treatment was acquired and analyzed by Joshua Solomon. The high throughput patch clamp study for danazol (data not shown) was conducted by Dr. Corey Valinsky. The above work has been labelled as "Results – Part B."

Data analysis – All data analysis was performed by the individuals whom collected the data, unless stated otherwise

References

Abbott GW, Sesti F, Splawski I, Buck ME, Lehmann MH, Timothy KW, Keating MT, Goldstein SA (1999). MiRP1 forms IKr potassium channels with HERG and is associated with cardiac arrhythmia. Cell 9, 175–187.

Adaixo R, Harley CA, Castro-Rodrigues AF & Morais-Cabral JH (2013). Structural properties of PAS domains from the KCNH potassium channels. PLoS ONE 8, e59265.

Anderson CL, Delisle BP, Anson BD, Kilby JA, Will ML, Tester DJ, Gong Q, Zhou Z, Ackerman MJ, January CT (2006). Most LQT2 mutations reduce Kv11.1 (hERG) current by a class 2 (trafficking-deficient) mechanism. Circulation 113, 365–373.

Apaja PM, Foo B, Okiyoneda T, Valinsky WC, Barriere H, Atanasiu R, Ficker E, Lukacs GL & Shrier A (2013). Ubiquitination-dependent quality control of hERG K+ channel with acquired and inherited conformational defect at the plasma membrane. Mol Biol Cell 24, 3787–3804.

Armstrong CM (1966). Time course of TEA(+)-induced anomalous rectification in squid giant axons. J Gen Physiol 50, 491–503.

Armstrong CM (1969). Inactivation of the potassium conductance and related phenomena caused by quaternary ammonium ion injection in squid axons. J Gen Physiol 54, 553– 575.

Armstrong CM (1971). Interaction of tetraethylammonium ion derivatives with the potas- sium channels of giant axons. J Gen Physiol 58, 413– 437.

Armstrong CM (1974). Ionic pores, gates, and gating currents. Q Rev Biophys 7, 179–210.

Carmeliet E (1992). Voltage- and time-dependent block of the delayed K current in cardiac myocytes by dofetilide. J Pharmacol Exp Ther 262, 809 – 817.

Chadwick DJ and Goode J (2005). The hERG Cardiac Potassium Channel: Structure, Function and Long QT Syndrome. Novartis Foundation Symposium 266.

Chen J, Zou A, Splawski I, Keating MT, and Sanguinetti MC (1999). Long QT syndrome associated mutations in the Per-Arnt-Sim (PAS) domain of HERG potassium channels accelerate channel deactivation. J Biol Chem. 274(15), 10113-10118.

Chen J, Zou A, Splawski I, Keating MT, and Sanguinetti MC (1999). Long QT syndrome-associated mutations in the Per-Arnt-Sim (PAS) domain of hERG potassium channels accelerate channel deactivation. J Biol Chem. 274, 10113-10118.

Chiamvimonvat N et al. (2017). Potassium currents in the heart: functional roles in repolarization, arrhythmias and therapeutics. J Physiol 595(7), 2229-2252.

Courtney KR (1975). Mechanism of frequency-dependent inhibition of sodium currents in frog myelinated nerve by the lidocaine derivative GEA. J Pharmacol Exp Ther 195, 225–236.

Curran M, Splawski I, Timothy K, Vincent G, Green E, Keating M (1995). A molecular basis for cardiac arrhythmia: HERG mutations cause long QT syndrome. Cell 80, 795– 803.

Dong H, Dunn J, Lytton J (2002). Stoichiometry of the cardiac Na^+/Ca^{2+} exchanger NCX1.1measured in transfected HEK cells. Biophys J. 83, 1945-1952.

FDA Pharm Classes anagrelide. https://www.accessdata.fda.gov/spl/data/5d35a45c-4cc4-4559-9b7f-10fb61dd0e44/5d35a45c-4cc4-4559-9b7f-10fb61dd0e44.xml (Accessed June 9, 2017).

Ficker E, Dennis AT, Wang L , Brown AM (2003). Role of the cytosolic chaperones Hsp70 and Hsp90 in maturation of the cardiac potassium channel HERG. Circ Res 92, e87–100.

Ficker E, Jarolimek W, Kiehn J, Baumann A, Brown AM (1998). Molecular determinants of dofetilide block of HERG K^+ channels. Circ Res 82, 386 –395.

Ficker E, Kuryshev YA, Dennis AT, Obejero-Paz C, Wang L, Hawryluk P, Wible BA, Brown AM (2004). Mechanisms of arsenic-induced prolongation of cardiac repolarization. Mol Pharmacol 66, 33– 44.

Foo B, Williamson B, Young J, Lukacs G, Shrier A (2016). hERG quality control and the long qt syndrome. J Physiol 594(9), 2469-2481.

Gianulis EC, Trudeau MC (2011). Rescue of aberrant gating by a genetically-encoded PAS (Per-Arnt-Sim) domain in several long QT syndrome mutant human ERG (hERG) potassium channels. J Biol Chem.

Goineau, S., Legrand, C., & Froget, G. (2012). Whole-cell configuration of the patch-clamp technique inthe hERG channel assay to predict the ability of a compound to prolong QT interval. Curr Protoc Pharmacol 10, 10-15

Gong Q, Anderson CL, January CT & Zhou Z (2002). Role of glycosylation in cell surface expression and stability of HERG potassium channels. Am J Physiol Heart Circ Physiol 283, H77–H84.

Gong Q, Stump MR & Zhou Z (2011). Inhibition of nonsense-mediated mRNA decay by antisense morpholino oligonucleotides restores functional expression of hERG nonsense and frameshift mutations in long-QT syndrome. J Mol Cell Cardiol 50, 223–229.

Gong Q, Zhang L, Vincent GM, Horne BD & Zhou Z (2007). Nonsense mutations in hERG cause a decrease in mutant mRNA transcripts by nonsense-mediated mRNA decay in human long-QT syndrome. Circulation 116, 17–24.

Grandi E, Sanguinetti MC, Bartos DC, Bers DM, Chen-Izu Y, Chiamvimonvat N, Colecraft HM, Delisle BP, Heijman J, Navedo MF, Noskov S, Proenza C, Vandenberg JI & Yarov-Yarovoy V (2017). Potassium channels in the heart: structure, function and regulation. J Physiol 595, 2209–2228.

Guo J, Massaeli H, Xu J, Jia Z, Wigle JT, Mesaeli N & Zhang S (2009). Extracellular K^+ concentration controls cell surface density of IKr in rabbit hearts and of the HERG channel in human cell lines. J Clin Invest 119, 2745–2757.

Gustina AS & Trudeau MC (2011). hERG potassium channel gating is mediated by N- and C-terminal region interactions. J Gen Physiol 137, 315–325.

Gutman GA, Chandy KG, Adelman JP, Aiyar J, Bayliss DA, Clapham DE,Covarriubias M, Desir GV, Furuichi K, Ganetzky B, Garcia ML, Grissmer S, Jan LY, Karschin A, Kim D, Kuperschmidt S, Kurachi Y, Lazdunski M, Lesage F, Lester HA, McKinnon D, Nichols CG, O'Kelly I, Robbins J, Robertson GA, Rudy B, Sanguinetti M, Seino S, Stuehmer W, Tamkun MM, Vandenberg CA, Wei A, Wulff H, Wymore RS. International Union of Pharmacology. XLI (2003). Compendium of voltage-gated ion channels: potassium channels. Pharmacol Rev 55, 583–586.

Hamilton KL, and Kiessling M (2006). DCEBIO stimulates Cl- secretion in the mouse jejnum. *Am J Physiol Cell Physiol*. 290(1), C152-164.

Hantouche C, Williamson B, Valinsky WC, Solomon J, Shrier A, and Young JC (2016). Bag1 promotes TRC8-dependent degradation of misfolded hERG potassium channels. J Biol Chem. n/a-n/a.

Harley CA, Jesus CSH, Carvalho R, Brito RMM, Morais-Cabral JH (2012). Changes in channel trafficking and protein stability caused by LQT2 mutations in the PAS domain of the HERG channel. PLOS one 7(3).

Hille B (1977).Local anesthetics: hydrophilic and hydrophobic pathways for the drug-receptor reaction. J Gen Physiol 69, 497–515.

HSDB anagrelide (2005). HSDS Databank Number: 7325. Web. https://toxnet.nlm.nih.gov/cgi-bin/sis/search2/f?./temp/~AiRGmm:1 (accessed on June 9, 2017).

HSDB Artesunic acid (2006). HSDS Databank Number: 7458. Web. https://toxnet.nlm.nih.gov/cgi-bin/sis/search2/r?dbs+hsdb:@term+@rn+@rel+88495-63-0. (accessed on June 7, 2017).

Ishii K, Nagai M, Takahashii, and Endoh M (2003). Dissociation of E-4031 from the HERG channel caused by mutations of an amino acid results in greater block in high stimulation frequency. Cardiovasc Res 57(3), 651-659.

Kamiya K, Niwa R, Mitcheson JS, Sanguinetti MC (2006). Molecular determinants of HERG channel block. Mol Pharmacol 69, 1709 –1716.

Ke Y, Hunter MJ, Ng CA, Perry MD, and Vandenberg JI (2014). Role of the Cytoplasmic N-terminal Cap and Per-Arnt-Sim (PAS) domain in trafficking and stabilization of K_v11.1 channels. J. Biol. Chem. 289 (20), 13782-13791.

Ke Y, Ng CA, Hunter MJ, Mann SA, Heide J, Hill AP, and Vandenberg JI (2013). Trafficking defects in PAS domain mutant K_v11.1 channels: roles of reduced domain stability and altered domain-domain interactions. Biochem J, 454, 69-77.

Keating MT & Sanguinetti MC (2001). Molecular and cellular mechanisms of cardiac arrhythmias. Cell 104, 569-580.

Kiehn J, Lacerda AE, Brown AM (1999). Pathways of HERG inactivation. Am J Physiol Heart Circ Physiol 277, H199 –H210.

Kirsch GE, Trepakova ES, Brimecombe JC, Sidach SS, Erickson HD, Kochan MC, Shyjka LM, Lacerda AE, and Brown AM (2004). Variability in the measurement of hERG potassium channel inhibition: effects of termperature and stimulus pattern. J Pharmacol Toxicol Methods 50(2), 93-101.

Lees-Miller JP, Duan Y, Teng GQ, Duff HJ (2000). Molecular determinant of high-affinity dofetilide binding to HERG1 expressed in Xenopus oocytes: involvement of S6 sites. Mol Pharmacol 57, 367–374.

Li Q, and Weina P (2010). Artesunate: The best drug in the treatment of severe and complicated malaria. *Pharmaceuticals (Basel)*. 3(7), 2322-2332.

Miranda P, Manso DG, Barros F, Carretero L, Hughes TE, Alonso-Ron C, Dom´ınguez P & de la Pen˜a P (2008). FRET with multiply labeled HERG K^+ channels as a reporter of the in vivo coarse architecture of the cytoplasmic domains. Biochim Biophys Acta 1783, 1681–1699.

Mitcheson JS, Chen J, Sanguinetti MC (2000). Trapping of a methanesulfonanilide by closure of the HERG potassium channel activation gate. J Gen Physiol 115, 229 –240.

Morais Cabral JH, Lee A, Cohen SL, Chait BT, Li M, Mackinnon R (1998). Crystal structure and functional analysis of the HERG potassium channel N terminus: a eukaryotic PAS

domain. Cell 95, 649 – 655.

Morimura K, Yamamura H, Ohya S, and Imaizumi Y (2006). Voltage-dependent Ca2+-channel block by openers of intermediate and smallconductane Ca2+-activated K+ channel in urinary bladder smooth muscle cells. J Pharmacol Sci. 100(3), 237-241.

NCBI anagrelide, National Center for Biotenchonology Information. PubChem Compound Database; CID=2182, https://pubchem.ncbi.nlm.nih.gov/compound/anagrelide#section=Top (accessed June 9, 2017).

NCBI artesunate, National Center for Biotenchonology Information. PubChem Compound Database; CID=60196289, https://pubchem.ncbi.nlm.nih.gov/compound/60196289#section=Top (accessed June 9, 2017).

NCBI DCEBIO, National Center for Biotenchonology Information. PubChem Compound Database; CID=656765, https://pubchem.ncbi.nlm.nih.gov/compound/dcebio#section=Top (accessed June 9, 2017).

Na-Bangchang K, Krudsood S, Silachamroon U, Molunto P, Tasanor O, Chalemrut K, Tangpukdee N, Matangkasombut O, Kano S, and Looareesuwan S (2004). The pharmacokinetics of oral dihydrostemesinin and artesunate in healthy Thai vounteers. *Southeast Asian K Trop Med Pub Health* 35(3), 575-582.

Neher E. (1992) Correction for liquid junction potentials in patch clamp experiments. Methods Enzymol., 2017, 123-131.

Ng CA, Hunter MJ, Perry MD, Mobli M, Ke Y, Kuchel PW, King GF, Stock D, Vandenberg JI (2011). The N-terminal tail of hERG contains an amphipathic alpha-helix that regulates channel deactivation. PLoS One 6, e16191.

Ng CA, Phan K, Hill AP, Vandenberg JI & Perry MD (2014). Multiple interactions between cytoplasmic domains regulate slow deactivation of Kv11.1 channels. J Biol Chem 289, 25822–25832.

Numaguchi H, Mullins FM, Johnson JP Jr, Johns DC, Po SS, Yang IC, Tomaselli GF, Balser JR (2000). Probing the interaction between inactivation gating and Dd-sotalol block of HERG. Circ Res 87, 1012–1018.

Paulussen, A., A. Raes, G. Matthijs, D. J. Snyders, N. Cohen, and J. Aerssens (2002). A Novel Mutation (T65P) in the PAS Domain of the Human Potassium Channel HERG Results in the Long QT Syndrome by Trafficking Deficiency. J Biol Chem. 277.50 : 48610- 8616.

Pedarzani P, McCutcheon JE, Rogge G, Jensen BS, Chistophersen P, Hougaard C, Strokbaek D, and Stocker M (2005). Specific enhancement of SK channel activity selectibely potentiates the afterhyperpolarizing current I(AHP) and modulates the firing properties of hippocampal pyramidal neurons. J Biol Chem. 280(50), 41404-41411.

Perrin MJ, Kuchel PW, Campbell TJ, Vandenberg JI (2008). Drug binding to the inactivated state is necessary but not sufficient for high-affinity binding to human ether-a-go-go-related gene channels. Mol Pharmacol 74, 1443–1452.

Perry MD, Ng CA, Mann SA, Sadrieh A,Imtiaz M, Hill AP, and Vandenberg JI (2015). Getting to the heart of hERG K^+ channel gating. J Physiol. 593(12), 2575-2585.

Perry MD, Ng CA, Phan K, David E, Steer K, Hunter MJ, Mann SA, Imtiaz M, Hill AP, Ke Y, and Vandenberg JI (2016). Rescue of protein expression defects may not be enough to abolish pro-arrhythmic phenotype of long QT type 2 mutations. J Physiol 594(14), 4031-4049.

Perry MD, Sanguinetti M, and Mitcheson J (2010). Revealing the structural basis of action of hERG potassium channel activators and blockers. J Physiol 588(17), 3157-3167.

Peterson LB, Eskew JD, Vielhauer GA & Blagg BS (2012). The hERG channel is dependent upon the Hsp90α isoform for maturation and trafficking. Mol Pharm 9, 1841–1846.

Petrecca K, Atanasiu R, Akhavan A & Shrier A (1999). N-linked glycosylation sites determine HERG channel surface membrane expression. J Physiol 515, 41–48.

Phartiyal P, Sale H, Jones EM & Robertson GA (2008). Endoplasmic reticulum retention and rescue by heteromeric assembly regulate human ERG 1a/1b surface channel composition. J Biol Chem 283, 3702–3707.

Piippo, Kirsi, Päivi Laitinen, Heikki Swan, Lauri Toivonen, Matti Viitasalo, Michael Pasternack, Kristian Paavonen, Hugh Chapman, Kenneth T. Wann, Eeva Hirvelä, Antti Sajantila, and Kimmo Kontula. (2000) Homozygosity for a HERG Potassium Channel Mutation Causes a Severe Form of Long QT Syndrome: Identification of an Apparent Founder Mutation in the Finns. Journal of the American College of Cardiology 35.7: 1919-925.

Piper DR, Hinz WA, Tallurri CK, Sanguinetti MC, Tristani-Firouzi M (2005). Regional specificity of human ether-a'-go-go-related gene channel activation and inactivation gating. J Biol Chem 280: 7206 –7217.

Piper RC, Dikic I & Lukacs GL (2014). Ubiquitin-dependent sorting in endocytosis. Cold Spring Harb Perspect Biol 6, a016808.

Rajamani, S., C. L. Anderson, B. D. Anson, and C. T. January (2002). Pharmacological Rescue

of Human K Channel Long-QT2 Mutations: Human Ether-a-Go-Go-Related Gene Rescue Without Block. Circulation 105.24: 2830-835.

Ramzy RM, Hafez ON, Gad AM, Faris R, Harb M, Buck AA, and Weil GJ (1994). Efficient assessment of filariasis endemicity by screening for filarial antigenaemia in a sentinel population. *Trans R Soc Trop Med Hyg*. 88(1), 41-44.

Robertson GA, January CT (2006) HERG trafficking and pharmacological rescue of LQTS-2 mutant channels. Handb Exp Pharmacol. pp 349–355.

Roden DM (2004). Drug-induced prolongation of the QT interval. N Engl J Med 350, 1013–1022.

Sale H, Wang J, O'Hara TJ, Tester DJ, Phartiyal P, He JQ, Rudy Y, Ackerman MJ, Robertson GA (2008). Physiological properties of hERG 1a/1b heteromeric currents and a hERG 1b-specific mutation associated with Long-QT syndrome. Circ Res 103, e81–95.

Sanders CR, Myers JK (2004). Disease-related misassembly of membraneproteins. AnnuRev Biophys Biomol Struct 33, 25–51.

Sanguinetti MC (2014). HERG1 channel agonists and cardiac arrhythmia. *Curr Opin Pharmacol*. 15, 22-27.

Sanguinetti MC, Jiang C, Curran ME, Keating MT (1995). A mechanistic link between an inherited and an acquired cardiac arrhythmia: HERG encodes the IKr potassium channel. Cell 81, 299 –307.

Sanguinetti MC, Jurkiewicz NK (1990). Two components of cardiac delayed rectifier K^+current Differential sensitivity to block by class III antiarrhythmic agents. J Gen Physiol 96, 195–215.

Sanguinetti MC, Tristani- Firouzi M (2006). hERG potassium channels and cardiac arrhythmia. Nature 440, 463– 469,

Schonherr R, Heinemann SH (1996) Molecular determinants for activation and inactivation of HERG, a human inward rectifier potassium channel. J Physiol 493(Pt 3), 635–642.

Schwartz PJ, Stramba-Badiale M, Crotti L, Pedrazzini M, Besana A, Bosi G, Gabbarini F, Goulene K, Insolia R, Mannarino S, Mosca F, Nespoli L, Rimini A, Rosati E, Salice P & Spazzolini C (2009). Prevalence of the congenital long-QT syndrome. Circulation 120, 1761–1767.

Sherman A. J., Shrier A., Cooper E. (1999). Series resistance compensation for whole-cell patch-clamp studies using a membrane state estimator. Biophys. J.77, 2590–2601.

Shushu L, Kerem B, Goldmit M, Peretz A, Attali B, Medina A, Towbin JA, Kurokawa J, Kass RS, and Benhorin J (2005) Clinical, genetic, and electrophysiological characteristics of a new PAS-domain HERG mutation (M124R) causing Long QT syndrome.

Singh S, Syme CA, Singh AK, Devor DC, and Bridges RJ (2001). Benzimidazolone activators of chloride secretion: potential therapeutics for cystic fibrosis and chronic obstructive pulmonary disease. *J Pharmacol Exp Ther*. 296(2), 600-611.

Smith PL, Baukrowitz T, Yellen G (1996). The inward rectification mechanism of the HERG cardiac potassium channel. Nature 379, 833– 836.

Sokoya EM, You K, and Chen J (2007). DCEBIO-mediated dilations are attenuated in the female rat middle cerevral artery. J Vasc *Res.* 44(3), 169-174.

Spector PS, Curran ME, Zou A, Keating MT, Sanguinetti MC (1996) Fast inactivation causes rectification of the IKr channel. J Gen Physiol 107, 611–619.

Stork D, Timin EN, Berjukow S, Huber C, Hohaus A, Auer M, and Hering S (2007). State dependent dissociation of HERH channel inhibitors. Br J Pharmacol 151(8), 1369-1376.

Strichartz GR (1973). The inhibition of sodium currents in myelinated nerve by quaternary derivatives of lidocaine. J Gen Physiol 62, 37–57.

Subbiah RN, Clarke CE, Smith DJ, Zhao J, Campbell TJ, Vandenberg JI (2004). Molecular basis of slow activation of the human ether-a-go-go related gene potassium channel. J Physiol 558, 417– 431.

Tan PS, Perry MD, Ng CA, Vandenberg JI, and Hill AP (2012). Voltage –sensing domain mode shift is coupled to the activcation gate by the N-terminal tail of hERG currents. J Gen Physiol. 140 (3), 293-306.

Troy S, Parks V, Purkayastha J, Gossart S, Goodman DB, Achenbach H, Armstrong M, and Martin PT (2014). Effect of anagrelide on cardiac repolarization in healthy volunteers: a randomized, double-blind placebo- and positive-controlled, thorough QT study. Pharmacol Res & Perspect 2(6), 2052-1707.

Trudeau MC, Warmke JW, Ganetzky B, Robertson GA (1995). HERG, a human inward rectifier in the voltage-gated potassium channel family. Science 269, 92–95.

Vandenberg JI, Perry MD, Perrin MJ, Mann SA, Ke Y, and Hill AP (2012) hERG K^+ channels: structure, function, and clinical significance. Physiol Rev 92, 1393-1478.

Wang L, Dennis AT, Trieu P, Charron F, Ethier N, Hebert TE, Wan X, Ficker E (2009). Intracellular potassium stabilizes human ether-a-go-go-related gene channels for ex- port

from endoplasmic reticulum. *Mol Pharmacol* 75, 927–937.

Wang DT, Hill AP, Mann SA, Tan PS, Vandenberg JI (2011). Mapping the sequence of conformational changes underlying selectivity filter gating in the K(v)11.1 potassium channel. Nat Struct Mol Biol 18, 35– 41.

Wang L, Wible BA, Wan X & Ficker E (2007). Cardiac glycosides as novel inhibitors of human ether-a-go-go-related gene channel trafficking. J Pharmacol Exp Ther 320, 525–534.

Waring MJ, Arrowsmith J, Leach AR, Leeson PD, Mandrell S, Owen RM, Pairaudeau G, Pennie WD, Pickett SD, Wang J, Wallace O & Weir A (2015). An analysis of the attrition of drug candidates from four major pharmaceutical companies. Nat Rev Drug Discov 14, 475–486.

Warmke JW, Ganetzky B (1994). A family of potassium channel genes related to eag in Drosophila and mammals. Proc Natl Acad Sci USA 91, 3438 –3442.

Witchel H, Milnes JT, Mitcheson JS, Hancox JC (2002). Troubleshooting problems with in vitro screening of drugs for QT interval prolongation using HERG K^+ channels expressed in mammalian cell lines and *Xenopus* oocytes. J. Pharmacol. & Toxicol Meth. 48(2), 65-80.

Yang BF, Xu DH, Xu CQ, Li Z, Du ZM, Wang HZ, Dong DL (2004). Inactivation gating determines drug potency: a common mechanism for drug blockade of HERG chan- nels. Acta Pharmacol Sin 25, 554 –560.

Yang T, Chun YW, Stroud DM, Mosley JD, Knollmann BC, Hong C & Roden DM (2014). Screening for acute I_{Kr} block is insufficient to detect torsades de pointes liability: role of late sodium current. Circulation 130, 224–234.

Yang T, Snyders DJ, Roden DM (1995). Ibutilide, a methanesulfonanilide antiarrhythmic, is a potent blocker of the rapidly activating delayed rectifier K current (IKr) in AT-1 cells. Concentration-, time-, voltage-, and use-dependent effects. Circulation 91, 1799– 1806.

Zhang L, Vincent GM, Baralle M, Baralle FE, Anson BD, Benson DW, Whiting B, Timothy KW, Carlquist J, January CT, Keating MT, Splawski I (2004). An intronic mutation causes long QT syndrome. J Am Coll Cardiol 44, 1283–1291.

Zhang M, Liu J, Tseng GN (2004). Gating charges in the activation and inactivation processes of the HERG channel. J Gen Physiol 124, 703–718.

Zhou J, Augelli-Szafran CE, Bradley JA, Chen X, Koci BJ, Volberg WA, Sun Z, and Cordes JS (2005). Novel potent human *ether-a-go-go*-related gene (hERG) potassium channel enhancers and their in vitro antiarrhythmatic activity. *Mol Pharmacol.* 68, 876-884.

Zhou Z, Gong Q, Epstein ML, January CT (1998). HERG channel dysfunction in human long

QT syndrome. Intracellular transport and functional defects. J Biol Chem 273, 21061–21066.

Zhou Z, Gong Q, January CT (1999). Correction of defective protein trafficking of a mutant HERG potassium channel in human long QT syndrome. Pharmacological and temperature effects. J Biol Chem 274, 31123–31126.

Zhou Z, Gong Q, Ye B, Fan Z, Makielski JC, Robertson GA & January CT (1998). Properties of HERG channels stably expressed in HEK 293 cells studied at physiological temperature. Biophys J 74, 230–241.